diversity

MDPI

Article

Scale-Dependent Drivers of Plant Community Turnover in a Disturbed Grassland: Insights from Generalized Dissimilarity Modeling

Zhengjun Wang *, Zhenhai Guan †, Liuhui Xu † and Sishu Zhao †

College of Life Sciences, Capital Normal University, Beijing 100048, China; 1160802057@cnu.edu.cn (Z.G.); 1150202029@cnu.edu.cn (L.X.); zhaosishu2016@126.com (S.Z.)

* Correspondence: wangzj@cnu.edu.cn

† The authors contributed equally to this work.

Abstract

Identifying the key drivers of plant community turnover under disturbance is essential for understanding ecological processes and informing conservation efforts. We investigated the Kangxi Grassland in the Yeyahu Wetland Nature Reserve, Beijing, using Generalized Dissimilarity Modeling (GDM) across two spatial scales and three areas, integrating soil properties, remote sensing data, and geographic distance. The models explained 25–49% of the deviance with low cross-validation error, showing a clear nonlinear turnover pattern. Pronounced species replacement occurred at short ecological distances, followed by slower change at greater distances. Although the overall patterns were similar, driver importance varied among areas: available nitrogen (AN) dominated in the Southeast Area, while soil water content (SWC) was the primary driver in the Northwest Area and across the entire Study Area; in all cases, geographic distance consistently ranked second. Texture indices, although weaker than geographic distance, still outperformed most vegetation indices and spectral bands. These results indicate that soil properties, geographic distance, and texture indices jointly shape spatial patterns of species turnover, with their relative importance varying by scale or area. Disturbances, such as drought, grazing, tourism, and fluctuations in inundated areas caused by variations in water levels in a nearby reservoir, influenced species turnover by directly or indirectly altering key drivers. In combination with a comparative analysis of species importance values (IVs) and ecological types, this study further demonstrates that the factors driving species turnover are influenced not only by scale but also by the complex and diverse ecological processes operating at their respective scales. It also shows the applicability of GDM in analyzing fine-scale turnover patterns and the factors driving them in disturbed grasslands.

Keywords: species composition; beta diversity; spatial patterns; environmental drivers; disturbance regime; community modeling

check for updates

Academic Editor: Mario A. Pagnotta

Received: 23 September 2025
Revised: 28 October 2025
Accepted: 6 November 2025
Published: 8 November 2025

Citation: Wang, Z.; Guan, Z.; Xu, L.; Zhao, S. Scale-Dependent Drivers of Plant Community Turnover in a Disturbed Grassland: Insights from Generalized Dissimilarity Modeling. *Diversity* **2025**, *17*, 786. https://doi.org/10.3390/d17110786

Copyright: © 2025 by the authors. Licensee MDPI, Basel, Switzerland. This article is an open access article distributed under the terms and conditions of the Creative Commons Attribution (CC BY) license (https://creativecommons.org/licenses/by/4.0/).

1. Introduction

In community ecology, beta diversity describes the rate or extent of species turnover along environmental gradients [1–4] and is typically quantified by comparing species composition between pairs of sites using similarity or dissimilarity indices [5–7]. While alpha diversity quantifies the diversity of species within individual sites, such as species richness [8,9], beta diversity quantifies compositional turnover between communities. This

turnover is typically assessed using indices such as Bray–Curtis dissimilarity, which captures shifts in species assemblages along environmental gradients [10,11]. By examining these compositional changes, beta diversity provides a more ecologically meaningful framework for understanding spatial and temporal patterns of biodiversity [12]. Due to its ecological importance, beta diversity has garnered considerable attention in biodiversity research [6]. Assessing spatial patterns of species turnover, linking community composition to environmental heterogeneity, and identifying the underlying gradients or drivers of species variation are essential for characterizing biodiversity hotspots and informing conservation and restoration strategies [13–16].

The similarity of species composition often declines with increasing distance, a pattern referred to as the distance–decay relationship [17–19]. This pattern has been observed across diverse taxa [20–23] and under varying environmental contexts [24,25], and its strength is highly scale-dependent [26]. Here, distance encompasses geographical [27,28], environmental [29,30], and spectral distances [31]. Geographical distance represents spatial factors and is commonly measured using Euclidean distance, which is generally associated with spatial autocorrelation among sites [32]. Environmental distance, also known as environmental dissimilarity, provides an integrative measure of how sites differ in environmental conditions, including factors such as climate, geomorphology, soil properties, and anthropogenic disturbances. Spectral distance quantifies differences among terrestrial habitats based on reflectance values in optical imagery [31,33–35] and serves both as an important tool for environmental monitoring and as an indicator and complement to geographic and environmental variables, enabling the assessment of spatial variability in environmental conditions captured by remote sensing data. Changes in beta diversity are often closely linked to both geographic distance and environmental gradients [36,37]. In practice, species turnover across ecological gradients arises from the combined effects of spatial and environmental processes [37,38]. This combined environmental influence reflects the underlying spatial heterogeneity of the environment, as greater ecological distance between sites indicates higher environmental heterogeneity, which in turn leads to greater community dissimilarity in species composition.

Several methods have been applied to describe the variation in species compositional similarity with distance. One straightforward and simple approach is ordinary least squares (OLS) regression, which establishes a linear model between species compositional similarity and the composite distance of environmental variables and infers the turnover rate or decay rate of species assemblages by analyzing the slope of the regression line [17,39,40]. Another approach employs quantile regression models [33], in which multiple high-quantile regressions are typically used to examine how species compositional similarity changes across different quantiles. However, both models have certain limitations when analyzing species turnover [41,42]. The general linear model describes the turnover rate across an entire region with a single slope, i.e., the average rate of change, whereas the quantile regression model, despite providing multiple slopes at different quantiles, can only capture several cross-sectional relationships between species turnover and environmental variation. Neither approach can fully explain how variations in environmental conditions influence species turnover rates. In fact, species turnover does not follow the linear patterns assumed by these models; instead, it exhibits nonlinear and continuous variation [[41–43].

Generalized Dissimilarity Modeling (GDM) relates species composition dissimilarity to ecological distance using nonlinear functions, allowing the detection of complex turnover patterns [12,42]. It also shows that the turnover rate of species composition changes continuously along environmental gradients [41,42,44] rather than being fixed at one or a few turnover rates [17,33,39,40]. This model was originally developed in the studies of Ferrier et al. [42,43,45] and later further programmed into an R package (gdm, version

1.6.0.7) [46]. The package provides a rich set of computational and analytical functions; it can not only analyze how species composition dissimilarity changes along environmental gradients or ecological distances, but also investigate the driving factors behind changes in species composition, determine the contribution or importance of variables, and predict the spatial distribution patterns of species composition [12]. The GDM framework has been widely applied across different scales, particularly in large-scale studies linking community compositional dissimilarity to ecological distance [41–43,47]. However, the use of this framework at the field scale remains limited, and little is known about species turnover under disturbance conditions, particularly in small-scale grassland environments affected by multiple disturbances such as drought, grazing, tourism, and fluctuations in water levels. Previous studies have primarily focused on climate variables [48,49], whereas remote sensing indicators remain less explored. Expanding GDM research to incorporate these factors would broaden the model's applicability.

To address the gaps in understanding plant community turnover in disturbed grasslands, we applied GDM at the plot level in the Kangxi Grassland of the Yeyahu Wetland Nature Reserve, Beijing, to analyze the effects of soil, remote sensing, and geographic distance variables on species turnover under multiple disturbance conditions. Our objectives were to (1) confirm the key determinants influencing the spatial patterns of species turnover across scales, (2) quantify the relative contributions of different categories of explanatory variables, (3) evaluate the effectiveness of remote sensing indicators for monitoring community dissimilarity, and (4) investigate the scale dependence of turnover drivers. By assessing the applicability of the GDM approach at the plot level, this study provides valuable methodological and theoretical insights for biodiversity conservation and restoration in disturbed grassland ecosystems.

2. Materials and Methods

2.1. Study Area

This study was conducted in the Kangxi Grassland within the Yeyahu Wetland Nature Reserve, Beijing, located in the experimental zone of the reserve (see Figure 1). The region has a continental monsoon climate with dry winters and springs, while summers and autumns are characterized by abundant sunshine and rainfall concentrated between July and September [50,51]. Historically, the area served as the Kangxi Grassland Tourist Area, within which grazing and tourism were prevalent [52]; however, the area is now under the administration of the Yeyahu Wetland Reserve, meaning grazing and tourism are strictly controlled and wetland restoration activities have been initiated. Nevertheless, during our fieldwork, we observed ongoing disturbance: about 28 horses regularly grazed in the grassland under managed care, and approximately 30 tourists visited daily for sightseeing and horseback riding. Rising water levels in the nearby Guanting Reservoir have also submerged large portions of former grassland, altering vegetation composition and structure in transitional zones near the inundated area.

To investigate scale dependence, the study area was divided into two nearly equal subareas—the Northwest and Southeast Areas—to represent the finer local scale, whereas the entire Study Area was considered the coarser scale. This yielded two spatial scales encompassing three areas in total (see Figure 1). The Northwest Area, adjacent to the inundated zone, is characterized by relatively moist soils, whereas the Southeast Area, near the entrance, has drier soils and a smaller amount of vegetation cover. The area is further crossed by trampled bare-soil paths and, overall, vegetation remains relatively short, except for taller *Artemisia tanacetifolia* communities near the entrance.

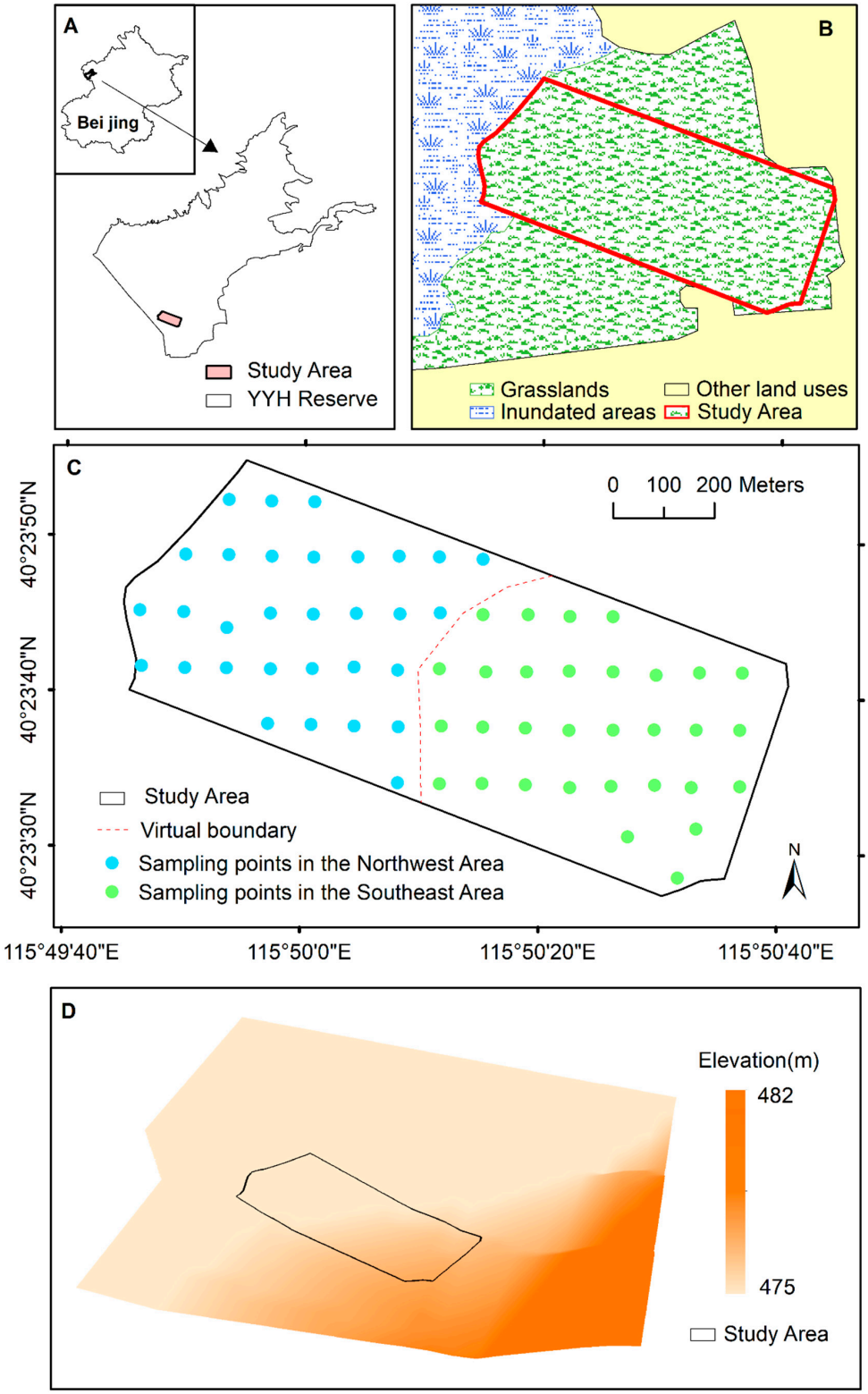


Figure 1. Location of the study area, sampling points, and their surrounding environment. (**A**) Location of the study area within Beijing and the Yeyahu Wetland Nature Reserve. (**B**) Surrounding environment of the study area. (**C**) Distribution of sampling points in the Northwest and Southeast Areas. The red dashed line indicates the artificial boundary distinguishing the two different environmental conditions: the Northwest Area and the Southeast Area. (**D**) Three-dimensional topographic map showing the study area and its surrounding regions. YYH Reserve = Yeyahu Wetland Nature Reserve.

2.2. Survey and Analysis of Plant Community and Soil Physicochemical Properties

Field surveys were conducted during the stable plant growth season (July–August 2019), and 62 sampling points were systematically established along a transect from the pasture entrance to the inundated area (see Figure 1). At each 1 m × 1 m plot, plant composition, abundance, and cover were recorded, and the coordinates and elevation of each sampling point were obtained using a GPS device (Qstar, Hi-Target, Guangzhou, Guangdong, China). Within each plot, a representative subplot was positioned as close to the center as possible, with dense or tall vegetation in some areas limiting exact placement. At this location, a soil subsample (approximately 30 cm × 30 cm) was collected from a soil depth of 0–20 cm using a spade to characterize the soil conditions of the plot. Prior to sampling, surface litter, undecomposed plant residues, and loose debris were carefully removed to avoid contamination from non-soil materials and to ensure that the collected samples represented the actual soil layer. The collected soil was crushed and thoroughly mixed, and about 1 kg of pure soil was placed into a sealed plastic bag. During sampling, disturbance to the vegetation and surrounding environment was minimized as much as possible.

In the laboratory, a portion of each soil sample was promptly weighed to determine fresh mass, then oven-dried at 105 °C to a constant weight to calculate the soil water content (SWC) [53,54]. The remaining soil was air-dried indoors for subsequent physicochemical analyses [53,54]. The air-dried soil underwent further processing prior to analysis. First, all naturally air-dried soil samples were passed through a 2 mm sieve, and approximately 200 g of the sieved soil was taken for determination of available nutrients and physical properties, including available nitrogen (AN), available phosphorus (AP), available potassium (AK), pH, electrical conductivity (EC), and soil texture. From this sieved portion, approximately 20 g was further passed through a 0.149 mm sieve; the fully sieved soil was used for analysis of total nutrients, including soil organic matter (SOM), total nitrogen (TN), total phosphorus (TP), and total potassium (TK).

Determination of SOM. Approximately 0.20 g of air-dried soil was placed in a dry hard-glass test tube and digested with 5 mL 0.8 mol L^{-1} $K_2Cr_2O_7$ and 5 mL concentrated H_2SO_4 in a liquid paraffin oil bath at 185–190 °C, boiled at 170–180 °C for 5 min, and then cooled. The digest was transferred to a 250 mL Erlenmeyer flask, 2–3 drops of 1,10-phenanthroline indicator were added, and titration was performed using 0.2 mol L^{-1} $FeSO_4$. Soil organic carbon (SOC) content was calculated using the Van Bemmelen factor (1.724) [53,54].

Determination of TN. Approximately 1.0 g of air-dried soil was digested with 2 g mixed catalyst (K_2SO_4:$CuSO_4$:Se = 100:10:1) and 5 mL concentrated H_2SO_4 in an automatic digestion system. After filtration, an aliquot was analyzed using a continuous flow analyzer (Auto Analyzer 3 System, SEAL Analytical GmbH, Germany).

Determination of TP. Approximately 0.5–1.0 g of air-dried soil was moistened and digested with 8 mL H_2SO_4 and 10 drops of 70–72% $HClO_4$ until the solution turned white, then boiled for 20 min. After cooling, the digest was diluted to 100 mL, and 5 mL of the supernatant was transferred to a 50 mL volumetric flask. The solution was diluted to about three-fifths of the volume, 2 drops of dinitrophenol indicator were added, and the pH was adjusted until the yellow color disappeared. Five milliliters of molybdenum–antimony reagent were added, and the samples was mixed, diluted to volume with water, and left at room temperature for 30 min before measuring phosphorus levels colorimetrically at 880 nm using a UV–Vis spectrophotometer (UV-2700, Shimadzu, Kyoto, Japan).

Determination of TK. Approximately 0.10–0.25 g of air-dried soil was weighed and placed in a PTFE digestion vessel. Five milliliters of ultrapure HNO_3 and 3 mL of ultrapure HF were added, and the vessel was subjected to microwave digestion (120 °C for 2 min, 180 °C for 15 min). After cooling, the digest was evaporated at 180 °C to less than 2 mL,

then diluted to 50 mL with ultrapure water. TK was determined by atomic absorption spectrophotometry (AA-6701F, Shimadzu, Japan).

Determination of AN. A total of 2 g of air-dried soil was placed in the outer chamber of a diffusion dish, with 2 mL of an indicator solution containing H_3BO_3 in the inner chamber. After sealing, 10 mL of 1 mol L^{-1} NaOH was added, and the dish was incubated at 40 °C for 24 h. The ammonia absorbed in the inner chamber was titrated with 0.005 mol L^{-1} H_2SO_4 standard solution until the color changed from blue to purple-red.

Determination of AP. About 2.5 g of air-dried soil was extracted with 50 mL of 0.5 mol L^{-1} $NaHCO_3$ (pH 8.5) containing phosphorus-free activated carbon at 25 °C for 30 min under shaking. The filtrate was reacted with molybdenum–antimony reagent, and phosphorus was measured colorimetrically at 880 nm (UV-2700, Shimadzu, Japan).

Determination of AK. A total of 5 g of air-dried soil was extracted with 50 mL of 1 mol L^{-1} ammonium acetate, shaken for 30 min, filtered, diluted 25-fold, and analyzed via atomic absorption spectrophotometry (AA-6701F, Shimadzu, Japan).

Determination of soil pH and EC. An amount of 5 g of air-dried soil was mixed with 25 mL CO_2-free deionized water, stirred for 1–2 min, and allowed to stand for 30 min, and the resulting supernatant was analyzed using a multiparameter water quality analyzer (DZS-706A, Shanghai Leici Instruments, Shanghai, China).

Determination of Soil Texture (Hydrometer Method). Soil texture was determined at 20 sampling points within a subset of plots across the study area, with one additional point located near the outer northern boundary of the Northwest Area. Uniformly air-dried soil samples weighing 50 g were placed in 500 mL Erlenmeyer flasks with 250 mL of distilled water. A suitable dispersing agent was added according to soil pH, and the suspension was shaken and allowed to stand for 2 h. The mixture was then gently boiled for 1 h on an electric hot plate while being frequently shaken to prevent soil particles from settling and forming aggregates at the bottom. Hydrometer readings were recorded at specified times and temperatures according to the standard relationship among temperature, sedimentation time, and particle size. Based on the mass percentages of sand (0.05–2.0 mm), silt (0.002–0.05 mm), and clay (<0.002 mm), the soil texture class was determined using the USDA soil texture classification triangle [55].

2.3. Remote Sensing Data

The satellite imagery was acquired from WorldView-2 (WV-2) on 7 September 2019 during clear, cloud-free weather conditions. The images underwent radiometric calibration, atmospheric correction, geometric correction, and image fusion processing. Geometric correction was performed with the support of ERDAS IMAGINE 9.2 (ERDAS, Norcross, GA, USA, 2008), with the correction error controlled within half a pixel. The other three processes were carried out with the support of ENVI 5.3.1 (Exelis Visual Information Solutions, Boulder, CO, USA, 2015). Specifically, atmospheric correction was performed using ENVI's FLAASH module. The study used the fused images with a spatial resolution of 0.5 m per pixel.

Vegetation indices (VIs) are indicators of plant growth and health [56] and are widely applied in biodiversity monitoring and modeling [57,58]. A total of 66 VIs were derived from WV-2 spectral bands (see Table A1), designed to capture vegetation growth, health, chlorophyll content, and soil moisture. VIs were calculated using the Raster Calculator in ArcGIS 10.2 (Esri, Redlands, CA, USA, 2013). In disturbed ecosystems, using single-date remote sensing to monitor vegetation diversity is often unreliable. To mitigate this limitation, we incorporated texture indices derived from WV-2 satellite imagery. Texture indices were calculated for each of the 8 spectral bands using the Gray-Level Co-occurrence Matrix (GLCM) method via the R package glcm. To identify the optimal spatial scale

compatible with our sampling design while maximizing model contribution, we computed indices across 5 window sizes (in pixels): 3 × 3, 5 × 5, 7 × 7, 9×9, and 11 × 11. The correlation texture index was excluded from subsequent analyses due to excessive missing values. Seven texture indices were retained for this study: mean, variance, homogeneity, contrast, dissimilarity, entropy, and angular second moment (ASM). This yielded 56 indices per scale (7 indices × 8 bands).

2.4. Statistical Analysis and Modeling

2.4.1. Species Importance Value and Ecological Types

The importance value (IV), an indicator reflecting the relative dominance of plant species within a community, was calculated as the mean of relative abundance, relative frequency, and relative coverage. Relative abundance, relative frequency, and relative coverage were determined as the proportions of each species' abundance, frequency, and coverage to the corresponding totals of all species [59]. Based on species IVs, the top 20 species in each area were analyzed according to their ecological type. The top-ranking species in each area were regarded as the dominant species of that area. Plant ecological type (mesophytic, hygrophytic, halophytic, and emergent) was classified following established references [60].

2.4.2. GDM and Evaluation

Species and environmental data were compiled at the level of individual sampling sites. The species dataset was formatted as a CSV file containing the species identity, geographic coordinates of the sampling plots, and species abundance. The environmental dataset was likewise prepared in CSV format, including the plot ID, coordinates, and corresponding environmental variables. For raster-derived variables, such as vegetation indices, values were extracted at the sampling locations. Geographic distance, treated as an additional predictor, was incorporated only in the final model simulations.

We applied GDM to simulate the patterns of species compositional dissimilarity along ecological distances, with the response variable being the Bray–Curtis dissimilarity index [61], calculated from abundance data after Hellinger transformation. Model performance was assessed using the percentage of deviance explained [41] as the primary criterion for goodness-of-fit, while cross-validation evaluated predictive accuracy and generalization capability. Variable contributions were quantified by summing I-spline coefficients, and Monte Carlo permutation determined their significance using 100 permutations, with a significance level of $p = 0.05$ [42,48]. Further validation included correlation analysis and *t*-tests between predicted and observed compositional dissimilarities. Due to the non-normal distribution of the data, a Monte Carlo permutation was conducted with 9999 permutations to assess the significance of the correlation and *t*-test results.

Compositional turnover along ecological gradients was quantified as the slope of predicted ecological distance versus the observed dissimilarity curves between consecutive points. Each slope, representing the turnover rate, was calculated as the ratio of dissimilarity change to ecological distance change. To compare regional turnover patterns, overlapping ecological distances were categorized into three intervals (0.6–1, 1–1.5, and 1.5–2), and the mean and standard deviation of slopes were computed for each interval, providing a standardized measure of spatial compositional change across environmental gradients.

2.4.3. Variable Selection Process

Based on the GDM framework described above, a four-step variable selection process was implemented to refine predictors and reduce redundancy.

1. Texture indices: For the five spatial scales of texture indices (excluding geographic distance), we fitted GDMs to examine their relationships with community compositional

dissimilarity. Based on the summed coefficients of the I-spline functions, variables with zero contribution were excluded, and the remaining predictors were retained to form a new set of texture indices [41,42].

2. Environmental and spectral variables: Using a similar approach, environmental variables (soil and elevation), eight spectral bands of WV-2 imagery, vegetation indices, and the texture indices with non-zero contributions from Step 1 were modeled separately. Variables with non-zero contributions from these models were retained, resulting in four sets of variables.

3. Joint modeling with geographic distance: The four variable sets were combined in a GDM including geographic distance. Variables with non-zero contributions were retained.

4. Final refinement: To reduce redundancy among the retained predictors, we further refined the variable set. Variables with negligible contributions were removed, highly correlated predictors ($|r| > 0.75$) were excluded [41], and multicollinearity was assessed using variance inflation factors (VIF > 10) [62]. Permutation test results were also considered, with predictors showing higher *p*-values being discarded. The remaining variables, together with geographic distance, were used for GDM, and the final set of significant predictors was employed in the ultimate simulation and for visualizing and decomposing variable contributions.

GDM construction, evaluation, cross-validation, variable selection, and contribution analysis were conducted using the gdm R package (version 1.6.0.7). Visualization and related statistical analyses, including *t*-tests, were performed in R (version 4.4.3, R Core Team, 2025). The map of the study area and sampling sites, as well as the three-dimensional (3D) topographic map, were generated using ArcGIS 10.2 (Esri, 2013). The 3D topographic map was created based on a 1:250,000-scale digital elevation model (DEM).

3. Results

3.1. Plant Community Composition and Distribution in the Three Areas

According to the statistics, the total number of species in the Study Area and its two subareas—the Southeast and Northwest Areas—are 65, 51, and 47, respectively, indicating that species richness is quite similar in the two subareas. In the Southeast Area, the two dominant plant species—*Artemisia tanacetifolia* and *Artemisia lavandulaefolia*—corresponding to the species with the highest IVs in this area (see Table A2), are both mesophytes. *Artemisia tanacetifolia* exhibits an aggregated distribution in some areas in the southern part of the Southeast Area, where disturbance is relatively intense. Despite this, cover and height remain high, indicating this species is the dominant plant community in these areas. In the Northwest Area, *Hemarthria altissima*, *Scirpus planiculmis*, *Artemisia tanacetifolia*, and *Inula japonica* are the dominant species (those with the highest importance values) and represent the typical plant communities in this area. *Hemarthria altissima* is a hygrophyte, *Scirpus planiculmis* is an emergent macrophyte, and *Artemisia tanacetifolia* and *Inula japonica* are mesophytes (see Table A3). In the marginal area, patchy communities of *Inula japonica* and *Scirpus planiculmis* are distributed, whereas *Typha angustifolia* and *Typha davidiana* communities extend from the edge of this subarea into the extensive outer inundated area. In the Study Area, the three principal plant communities are *Scirpus planiculmis*, *Hemarthria altissima*, and *Artemisia tanacetifolia* (see Table A4), corresponding to emergent, hygrophytic, and mesophytic species, respectively.

Considering the top 20 species by IVs in each of the three areas (where the sum of IVs exceeds 80%), the Northwest Area harbors a greater number of hygrophytic and emergent species than the Southeast Area. However, the IVs of these species are more pronounced in the Northwest Area (see Table 1). Although the number of hygrophytic and emergent species in the Northwest Area is only about half that of mesophytes, their cumulative IVs

are nearly equal. In the Southeast Area, mesophytic species are noticeably higher than the combined total of hygrophytic and emergent species, whether in species number or in IV. In the Study Area, mesophytes likewise exceed the sum of hygrophytic and emergent species in terms of both richness and IV (see Table 1). Moreover, two to three halophytic species occur in each area [60]; these species exhibit relatively high tolerance to drought and salinity [63].

Table 1. Number and cumulative IVs of different ecological types among the top 20 species in the three areas.

Areas	Mesophytes	Hygrophytes	Emergent Plants	Halophytes	Total
Southeast Area	13(60.9)	2(8.3)	2(7.9)	3(6.2)	20(83.3)
Northwest Area	12(42.2)	2(20.9)	4(20.8)	2(6.2)	20(90.1)
Study Area	13(46.6)	1(14.2)	3(17.9)	3(8.0)	20(86.7)

Note: Values in parentheses represent cumulative IVs (%).

3.2. Comparison of Soil Properties Between the Two Subareas

The comparison of soil properties between the two subareas revealed clear spatial differences (see Table 2). The *t*-test results indicated that SWC in the Southeast Area was significantly lower than that in the Northwest Area, while EC was also significantly smaller in the Southeast Area. In contrast, the AK content was significantly higher in the Southeast Area than in the Northwest Area. No significant differences were detected in the other soil variables between the two subareas.

Table 2. Comparison of soil properties between the two subareas (*t*-test).

Parameters	Southeast Area	Northwest Area	Significance
SOC	9.75 ± 5.17	8.33 ± 2.06	
SOM	16.80 ± 8.92	14.35 ± 3.55	
TN	0.93 ± 0.44	0.83 ± 0.20	
AN	0.06 ± 0.02	0.06 ± 0.01	
TP	0.44 ± 0.04	0.42 ± 0.04	
AP	0.01 ± 0.00	0.01 ± 0.00	
TK	18.54 ± 1.07	18.78 ± 2.09	
AK	0.21 ± 0.11	0.15 ± 0.05	**
SWC	0.07 ± 0.02	0.13 ± 0.05	***
pH	9.13 ± 0.13	9.05 ± 0.25	
EC	110.42 ± 15.28	419.52 ± 257.93	***

Note: ** indicates $p < 0.05$, *** indicates $p < 0.01$. The unit of EC is μS/cm; SWC is expressed as a ratio; pH has no unit; and all other soil properties are expressed in g/kg. The full names corresponding to the abbreviations of soil properties are provided in the Materials and Methods section.

Soil texture analysis indicated that among the 21 sampling points, 10 were classified as sandy loam and the rest as loam. Of the sandy loam sites, four were located in the Northwest Area and five in the Southeast Area, with one positioned near the outer northern boundary of the Northwest Area. The number of sandy soil points was roughly similar in both subareas, and their distribution exhibited a clustered but discontinuous pattern. In addition, six of the sandy loam points were situated near the exposed pathway running through the Southeast and Northwest Areas. Areas subject to greater disturbance tended to have more sandy soils, with the most pronounced sandiness generally observed along the pathway.

3.3. Model Evaluation

All three GDM models explained over 25% of the deviance (see Table 3), with the Northwest Area showing the highest values and the Study Area the lowest. The *t*-test

results revealed no significant differences between observed and predicted species dissimilarities for each area (all p-values > 0.05). Moreover, correlations between observed and predicted values were consistently high across all scales ($p < 0.01$; see Table 3; see Figure 2a,b, Figure 3a,b, and Figure 4a,b). These results indicate that the models provide consistent, unbiased predictions and account for a relatively high proportion of the variation in species turnover. Cross-validation further showed relatively low prediction errors for all three models (see Table 3). Although the proportion of deviance explained was generally higher in the training sets than in the test sets, all models accounted for more than 20% of the deviance across both datasets, and the small discrepancies between training and test sets suggest that the models generalize across datasets.

Table 3. Evaluation of GDM model performance for the Northwest Area, Southeast Area, and Study Area.

Metrics	Northwest Area	Southeast Area	Study Area
DE (%)	49.34	34.66	25.39
Intercept	0.44	0.51	0.58
Obs–Pred Corr	0.72 **	0.60 **	0.52 **
TDE (%)	38.48	33.82	25.7
TSTDE (%)	38.26	27.84	20.23
MPE	0.02	0.02	0.01
MAE	0.10	0.11	0.12
RMSE	0.13	0.13	0.15

Note: DE (Percent Deviance Explained) denotes the proportion of deviance explained by the model. Obs–Pred Corr is the correlation coefficient between observed and predicted species composition dissimilarities. TDE and TSTDE indicate the proportion of deviance explained for the training and test sets, respectively. MPE (Mean Prediction Error) is the average difference between predicted and observed values, MAE (Mean Absolute Error) is the mean of absolute differences, and RMSE (Root Mean Square Error) is the square root of the mean squared error. Bold values indicate cross-validation results; ** denotes significance at $p < 0.01$.

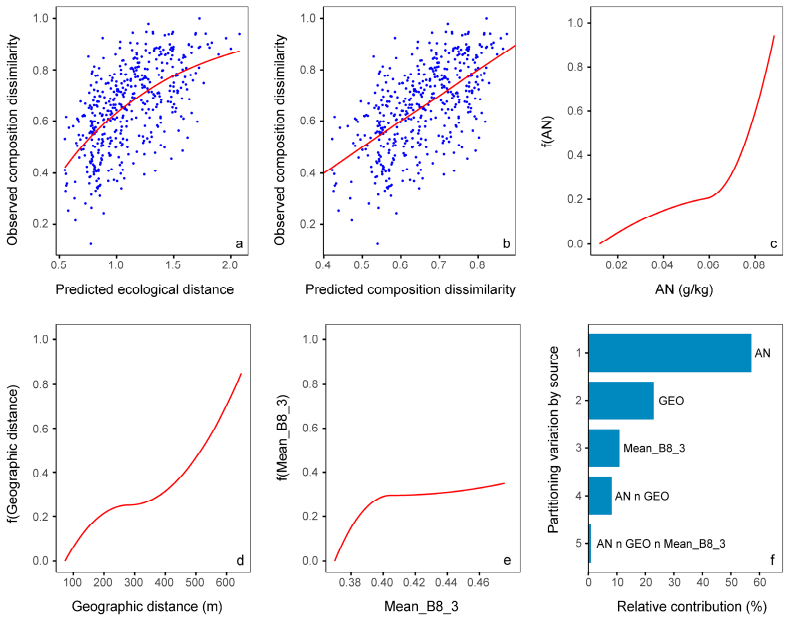


Figure 2. GDM results for the Southeast Area, including (**a**) the relationship between predicted ecological distance and observed species dissimilarity, (**b**) the relationship between predicted and observed dissimilarity (1:1 reference line in red), (**c**–**e**) I-spline responses for soil available nitrogen (AN), geographic distance, and Mean_B8_3 (a texture index derived from WorldView-2 imagery, representing the mean of Band 8 computed over a 3 × 3 window), and (**f**) the relative contributions of significant variables to the total deviance explained.

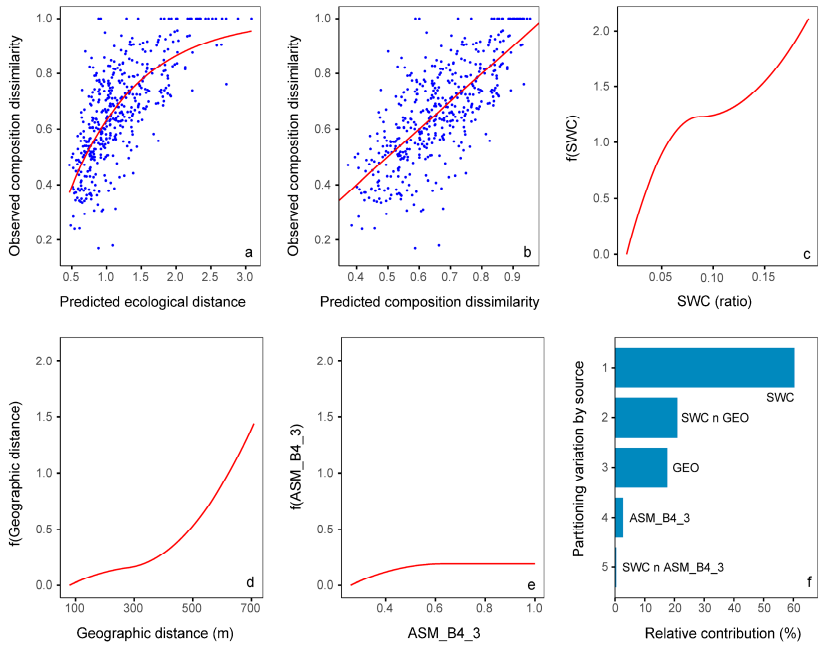


Figure 3. GDM results for the Northwest Area, including (**a**) the relationship between predicted ecological distance and observed species dissimilarity, (**b**) the relationship between predicted and observed dissimilarity (1:1 reference line in red), (**c**–**e**) I-spline responses for soil water content (SWC), geographic distance, and ASM_B4_3 (a texture index derived from WorldView-2 imagery, representing the Angular Second Moment of Band 4 computed over a 3 × 3 window), and (**f**) the relative contributions of significant variables to the total deviance explained.

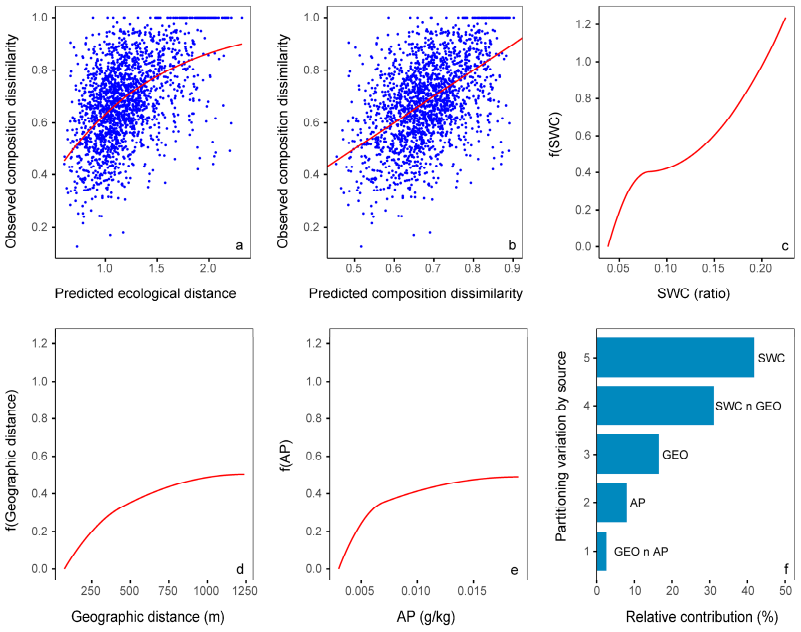


Figure 4. GDM results for the Study Area, including (**a**) the relationship between predicted ecological distance and observed species dissimilarity, (**b**) the relationship between predicted and observed dissimilarity (1:1 reference line in red), (**c**–**e**) I-spline responses for SWC, geographic distance, and available phosphorus (AP), and (**f**) the relative contributions of significant variables to the total deviance explained.

3.4. Patterns of Species Turnover

GDM simulations (see Figures 2a, 3a and 4a) showed that species composition in the three areas responded to environmental gradients with similar nonlinear patterns.

Turnover rates consistently decreased from lower to higher ecological distances, with values at short distances being more than twice those at long distances, while slopes in the intermediate range were nearly identical across areas (see Table 4). Differences in turnover rates among the three areas were small within all distance intervals, and standard deviations indicated little variation between adjacent points, suggesting stable turnover rates across ecological distances.

Table 4. Species turnover rates across the three areas.

Areas	Intervals	Average Turnover Rate (Slope)	Standard Deviation
Southeast Area	0.6–1	0.43	0.04
	1–1.5	0.30	0.04
	1.5–2	0.20	0.02
Northwest Area	0.6–1	0.45	0.05
	1–1.5	0.30	0.04
	1.5–2	0.18	0.03
Study Area	0.6–1	0.42	0.04
	1–1.5	0.31	0.04
	1.5–2	0.18	0.03

Overall, species dissimilarity exhibited highly consistent patterns across the three areas. Turnover rates peaked at short ecological distances and decreased nonlinearly toward longer distances, indicating that compositional turnover declines along environmental gradients.

Ecological distance ranges differed among areas: Southeast Area, 0.55–2.00 (span = 1.45); Study Area, 0.60–2.22 (span = 1.62); Northwest Area, 0.47–2.89 (span = 2.42). The Southeast Area had the narrowest range, indicating smaller pairwise differences, whereas the Northwest Area spanned the broadest range, encompassing the values of the other two areas and extending beyond them, reflecting greater environmental heterogeneity and a stronger gradient.

3.5. Relative Importance of Variables

In the Southeast Area, AN (57.2%) and geographic distance (22.9%) are the main drivers, considerably exceeding the contribution of the texture index Mean_B8_3 (11%) to the total deviance explained (see Tables 3 and 5; see Figure 2c–f). In the Northwest Area, SWC dominates (59.2%), followed by geographic distance (17.2%), together accounting for ~76.4% of the explained deviance, whereas ASM_B4_3 contributes only ~2.7% (see Tables 3 and 5; see Figure 3c–f). Across the Study Area, SWC remains the most influential variable (41.8%), followed by geographic distance (16.5%) and AP (~8%), with the first two variables explaining ~58.3% of the total explained deviance (see Tables 3 and 5; see Figure 4c–f). The variable contribution rankings are fully consistent with the summed I-spline coefficients across all areas.

Table 5. Relative importance of variables across the three areas.

Variables	Southeast Area	Northwest Area	Study Area
SWC		2.13 **	1.25 **
GEO	0.86 **	1.46 **	0.50 **
AN	0.96 **		
Mean_B8_3	0.35 *		
AP			0.49 *
ASM_B4_3		0.19 *	

Note: SWC, AN, AP, and GEO denote soil water content, available nitrogen, available phosphorus, and geographic distance, respectively. Mean_B8_3 and ASM_B4_3 are texture indices derived from WorldView-2 imagery (WV-2), computed over a 3 × 3 window, with Mean_B8 representing the mean of the 8th band and ASM_B4 representing the Angular Second Moment of the 4th band. * and ** denote significance at $p < 0.05$ and $p < 0.01$, respectively.

4. Discussion

4.1. Influence of Soil Properties on Plant Community Composition and Distribution

According to the analysis (see Tables 2 and 5; Figures 3c and 4c), SWC exerts a significant influence on the composition and distribution of plant communities. Reflecting this environmental factor, the Northwest Area supports more hygrophilous species, with several tall emergent plants occurring near the edge of the inundation areas, while the Southeast Area is dominated by mesophytic species. This difference becomes even more apparent when considering the IVs (see Tables 1, A2 and A3). The simulation results of the GDM model also indicate that variation in SWC, both in the Northwest Area and across the Study Area (see Table 5), constitutes a key environmental gradient that strongly influences changes in plant community composition (see Table 5; see Figures 3c and 4c). SWC is closely related to both the elevational difference between the two subareas (elevation in the Southeast Area was significantly higher than in the Northwest Area, *t*-test, $p < 0.05$) and fluctuations in reservoir water levels. The Northwest Area, situated at a lower elevation near the inundation areas, has significantly higher SWC than the Southeast Area, resulting in distinct differences in community composition and ecological adaptation types (see Tables 1, A2 and A3).

The other two properties, EC and AK, also differ significantly between the two subareas (see Table 2). However, their contributions to species compositional dissimilarity were relatively minor in models involving either the subareas or the Study Area. In the GDM models for each subarea, the contribution of EC was consistently lower than that of AK and was excluded in the earlier stages of model simulation, while AK was also ultimately not included as a predictor in the final model due to a lack of significance in the later stages. In contrast, AN and AP did not differ significantly between the two subareas (see Table 2), yet they contributed significantly to species compositional dissimilarity in models for the Southeast Area or the Study Area as a whole (see Table 5; see Figures 2c and 4e). This indicates that these two variables form environmental gradients that strongly influence species turnover within their respective areas.

Compared with climatic variation, local-scale disturbances—such as fluctuations in water levels—had a more pronounced effect. At fine spatial scales, such as in the present study, the impacts of climate change are relatively uniform, whereas local disturbances exert distinct and substantial influences. In the Southeast Area, soil and plant community conditions have developed under the combined influence of long-term climatic factors, including drought [50,51], and human disturbances, such as grazing, while the Northwest Area experiences additional direct disturbance from fluctuating water levels, leading to pronounced differences in SWC and, consequently, variation in plant community composition and structure.

Soil texture analysis revealed that sandy soils exhibited a clustered yet discontinuous spatial pattern, indicating the widespread occurrence of soil sandification in the area. This sandification is closely associated with human disturbances. Activities such as trampling paths and grazing reduce vegetation cover, leaving soil exposed to weathering and facilitating sandification. The fine fractions of these sandy, degraded soils are easily eroded, washed away, or transported by wind and water. Some halophytic species (salt- and drought-tolerant plants) occurred throughout the study area (see Tables 1 and A2–A4), serving as indicators of these sandy, degraded habitats [60,63].

4.2. Relationship Between the Proportion of Deviance Explained by GDM and Explanatory Variables

The deviance explained by the GDM model was closely related to the number of variables included. When more variables with relatively high (though not strictly statisti-

cally significant) explanatory potential were incorporated, the overall deviance explained increased. In the initial stage, combining soil, geographic, and remote sensing predictors resulted in models with more than 19 variables that explained a relatively high proportion of deviance (see Table 6). After excluding low-contributing, highly correlated, or redundant variables, the number of explanatory variables decreased to ten or fewer, and model performance declined accordingly. In the final models, only significant variables were retained as predictors, as they provided stable contributions, consistent with previous studies [41]. Each final model retained three predictors, simplifying field preparation and monitoring while maintaining acceptable performance. The deviance they explained ranged from 25% to 49% (see Table 3), which aligns with the typical range reported for GDM [12]. These models also captured key gradients and compositional dissimilarity patterns without the uncertainty and effort associated with larger predictor sets, which is particularly important under disturbance conditions. Comparing models with different numbers of predictors reveals the trade-offs among predictor availability, model simplicity, and the proportion of deviance explained. In addition, the total deviance explained by the model was found to be influenced by the number of plots [12]; the increased number of plots resulted in a reduction in proportion of deviance explained for the Study Area as a whole (see Tables 3 and 6). This reduction is likely attributable to the greater complexity and uncertainty intrinsic to disturbed environments when using larger sample sizes, which in turn diminishes the explanatory capacity of the associated predictors, thereby reflecting the scale dependence of the deviance explained by GDM models.

Table 6. Effect of number of variables on the proportion of deviance explained by the GDM model.

Areas	Model Summary	Final Model 1	Final Model 2	Final Model 3
Study Area	Number of variables	25	8	3
	Deviance explained %	33.9	31.4	25.4
	Significant variables	SWC, GEO, AN, AP	SWC, GEO, AP	SWC, GEO, AP
Southeast Area	Number of variables	19	9	3
	Deviance explained %	47.3	44.0	34.7
	Significant variables	AN, GEO, TK, Entropy_B8_11	AN, GEO, Mean_B8_3	AN, GEO, Mean_B8_3
Northwest Area	Number of variables	26	10	3
	Deviance explained %	59.3	54.5	49.3
	Significant variables	SWC, GEO, Contrast_B8_3	SWC, GEO, ASM_B4_3 *	SWC, GEO, ASM_B4_3

Notes: GEO represents geographic distance. Contrast_B8_3 is a WV-2 texture index representing the contrast of band 8, calculated over a 3 × 3 window, while Entropy_B8_11 refers to the entropy of band 8 calculated over an 11 × 11 window. Abbreviations for other variables can be found in Table 5 or Section 2. Final Models 1, 2, and 3 illustrate the sequential processes in which soil factors, vegetation indices, texture indices, and WV-2 spectral bands were individually screened and then integrated for further simulation and variable selection, with Final Model 3 representing the study's ultimate model. * The variable with $p = 0.06$ was retained as it was close to statistical significance.

4.3. Similar Patterns Arise from Different Driving Mechanisms

In all three areas, species compositional dissimilarity increases with ecological distance, while the turnover rate continuously decreases and approaches stability. The shapes of the curves are highly similar, as are the turnover rates (see Table 4; see Figures 2a, 3a and 4a). These findings suggest that species compositional dissimilarity exhibits similar variation patterns across the three areas. However, further analysis revealed that the driving factors and their relative contributions to these distribution patterns differ among the areas. Although the Northwest and Southeast Areas are at the same spatial scale, their environments differ markedly. In the Northwest Area, located near a reservoir, large swaths of land are frequently submerged by water. Due to the alternating dry and wet seasons, some sites experience repeated periods of inundation and drying. This results in a higher SWC,

which promotes better plant growth. SWC is thus the dominant driving factor in this area, followed by geographic distance, which also significantly contributes to compositional dissimilarity (see Table 5; see Figure 3f). In the Southeast Area, soils are generally dry and deficient in water; therefore, SWC is not the main factor shaping vegetation composition. Instead, AN and geographic distance are the two most important factors influencing species compositional dissimilarity in this area (see Table 5; see Figure 2f). In such arid conditions, it is difficult for litter and organic matter to decompose into plant-available nutrients. Decomposed nutrients therefore become the limiting resource and key environmental gradient. At the Study Area scale, SWC is the dominant factor, while geographic distance and AP contribute to similar, though less strong, levels (see Table 5; see Figure 4f). SWC exhibits a clear gradient and trend throughout the two subareas, significantly constraining plant growth and species composition variation.

There are several reasons why different mechanisms may generate similar dissimilarity patterns. First, the observed patterns may reflect the combined effects of these key factors and other, as yet unidentified, drivers. Second, the environmental gradients of the two subareas (Northwest and Southeast Areas) may constitute parts of broader gradients present at larger scales. In addition, both subareas have experienced analogous long-term grazing and tourism disturbances, which are recognized as a driver of biotic homogenization [15]. The hypothesis that homogenization may partly account for the observed consistency in compositional dissimilarity patterns warrants further investigation.

Large-scale studies have shown that spatial patterns of species composition vary and that the ecological processes and primary gradients driving these patterns differ [41]. Our field-scale study demonstrates that, even when patterns appear similar, they may arise from different ecological processes. This finding suggests that the spatial patterns of species composition are contingent not only on scale but also on the complex and diverse ecological processes that vary across these scales [64,65].

4.4. The Role of Geographic Distance at Different Spatial Scales

At the regional scale, geographic distance reflects spatial isolation and dispersal limitations, such as barriers imposed by bodies of water or mountains, and habitat filtering due to climatic constraints [49]. Previous studies have shown that the explanatory power of geographic distance depends on the scale of investigation, taxonomic group, geographic context, historical climatic dynamics, and environmental complexity [16,22,41,66]. At finer spatial scales, however, geographic distance is more closely associated with habitat suitability or filtering. In our relatively flat study system, local factors, such as grazing and disturbances caused by fluctuations in reservoir water levels, produced site-level variation in SWC and AN, which represented key gradients shaping species composition and turnover.

Although geographic distance is strongly correlated with environmental variables, it should not be discounted. Geographic distance is an indicator of environmental heterogeneity and captures spatial structure that is not explained by other predictors [32]. The findings of the present study demonstrate that incorporating geographic distance into the model leads to a substantial enhancement in performance metrics across all three areas. This indicates that geographic distance is a key factor in the model framework (see Table 5; see Figures 2f, 3f and 4f). In GDM model studies, geographic distance, as a spatial variable, is a component of ecological distance. It works together with other variables to influence and explain the spatial patterns of species composition dissimilarity [16,41].

4.5. The Role of Remote Sensing Variables

We used eight spectral bands from WV-2 imagery, along with vegetation and texture indices, as explanatory variables when constructing the GDM. All three categories of remote sensing variables contributed to the models, though to varying degrees (see Table 7). When analyzed separately, the texture indices yielded different levels of deviance explained in the GDM across the three study areas and five spatial scales, with 56 indices included at each scale. The deviance explained was lowest in the Southeast Area and highest in the Northwest Area. In the Northwest Area, texture indices exhibited a greater capacity to explain the observed variation when compared to the Study Area, and this capacity was more than double that observed in the Southeast Area. Across all areas, the 3 × 3 scale consistently showed the highest deviance explained among the five scales. When the texture indices selected across all five scales were recombined and included in the GDM, the proportion of deviance explained by the model improved across all study areas (see Table 7). When 66 vegetation indices (see Table A1) and the eight WV-2 spectral bands were included, the WV-2 bands consistently explained a lower proportion of deviance than the vegetation and texture indices (see Table 7). At both the Northwest Area and Study Area scales, the contributions of the selected texture and vegetation indices were highly comparable within each scale. However, in the Southeast Area, the selected texture indices remained relatively strong predictors. While all three categories of remote sensing variables contributed to the models to a certain extent, their effects were not statistically significant.

Table 7. Percentage deviance explained by remote sensing variables (geographic distance excluded).

Areas	Texture Indices (Scales)					Selected Texture Indices	VI	WV-2
	3 × 3	5 × 5	7 × 7	9 × 9	11 × 11			
Study Area	18.9	18.0	18.0	18.0	18.2	19.2	19.5	18.0
Southeast Area	12.6	9.6	10.4	11.1	12.5	16.5	11.1	10.2
Northwest Area	29.2	26.4	24.1	25.1	25.4	32.0	31.8	22.0

Note: VI refers to the Vegetation Index. Deviance explained values in the table are given as percentages.

Although remote sensing variables contributed to model interpretation to varying degrees across different scales, the GDM model for the Southeast Area retained the statistically significant Mean_B8_3 texture index, whereas the model for the Northwest Area retained the significant ASM_B4_3 texture index. However, under disturbed environmental conditions, these indices explained much less deviance and were less important predictors than SWC and geographic distance. Nevertheless, the retention of these texture indices in the final models indicates that they outperformed many other candidate variables excluded during model selection. This suggests that texture indices can outperform vegetation indices and raw spectral bands, indicating that they can be valuable indicators and meaningful explanatory variables under disturbed environmental conditions.

Remote sensing is a powerful monitoring tool that provides rich, timely data in support of biodiversity monitoring, spatial analysis, and conservation efforts [67,68]. Remote sensing data are now widely used in scientific research and management practices [69,70]. However, in studies of beta diversity, remote sensing variables are rarely used as explanatory factors, possibly due to the large spatial scales involved and the difficulty of aligning remotely sensed and field-based data [71,72]. At finer spatial scales, however, using remote sensing variables becomes more feasible and provides additional data to help explain and predict species compositional dissimilarity.

4.6. Effects of Disturbance on Monitoring

In much of the study area and adjacent grasslands, especially in the southeast, the main disturbances are low-intensity grazing, tourism, and prolonged drought. In contrast,

reservoir water-level fluctuations dominate in the northwest. These disturbances have resulted in dry soils with patchy bare surfaces in many areas and, in some places, even soil desertification. Due to grazing, trampling by livestock and tourists, and drought, vegetation height and cover are generally low. The biophysical and biochemical cycles of plants are often disrupted, and the distribution of vegetation tended toward homogenization [15]. In the Southeast Area, mesophytic species such as Artemisia tended to aggregate and expand (see Table A2). At a broader spatial scale, the Study Area serves as a representative transect of the Kangxi Grassland and, in terms of soil types—sandy loam and loam exhibiting a clustered but discontinuous spatial pattern, also partially confirmed by a sandy loam site near the outer boundary of the Northwest Area—and plant composition, broadly reflects the conditions of the grassland.

Persistent disturbances introduced uncertainties and challenges to monitoring, including remote sensing-based monitoring. Aspects related to vegetation biomass, such as height and cover, are more susceptible to disturbance, while the physicochemical properties of the soil and plant species richness remain relatively stable over shorter time periods. Remote sensing images of land cover are usually captured at specific moments during satellite overpasses and may change rapidly due to temporal variations and disturbances. If a substantial time gap exists between the satellite overpass and the sampling time, the acquired images may not accurately reflect the survey data. This discrepancy can lead to considerable errors and hinder effective monitoring, particularly when monitoring biomass factors such as vegetation cover. This is a common challenge for remote sensing in disturbed environments. Conversely, species richness and abundance can be reliably determined within shorter time frames. Therefore, it is essential to minimize the temporal gap between the sampling and satellite overpass and to complete field sampling quickly to reduce errors caused by disturbance-related uncertainties. Furthermore, sampling should be conducted in the fall, when plants are in are relatively stable growth stage, rather than during the early germination stage. During this period, grazed grasses can still be identified and recorded, thereby maximizing the accuracy of plant diversity assessments.

In disturbed environments, the factors and ecological processes that drive vegetation dynamics also shift. In this study, common vegetation indices such as the NDVI did not explain a significant proportion of deviance, whereas texture indices such as Mean_B8_3 were retained in the models. Similarly, while certain soil variables, such as SOM and TN, showed no significant effects, SWC and available nutrients were identified as key environmental gradients.

For remote sensing monitoring under disturbed conditions, some studies use images from different time points for comparative analysis. This method is helpful for distinguishing and revealing locations or areas with anomalous changes [73,74]. However, there is limited research on the spatial patterns of plant species composition dissimilarity at the field scale. In our study, we used single-date WV-2 imagery because local management imposed strict control over grazing and tourism activities. In addition, using satellite images from a single time point also accounts for issues related to the longer ground sampling periods and the uncertainty of satellite overpasses, which affect data acquisition and matching. Our results show that even remote sensing monitoring at a single time point can reliably identify the patterns and driving forces of community composition variation under disturbed conditions.

4.7. Scale Dependence of the GDM Model

The GDM model's scale dependence is reflected at multiple levels: (1) The adaptability of variable granularity. This study used 0.5-m WV-2 remote sensing imagery as the source of remote sensing variables to align with the 1 × 1-m ground sampling scale. Compared to

multispectral imagery with a resolution of 2 m, the 0.5 m pan-sharpened WV-2 imagery provides a finer representation of the distribution and variation in plant diversity. In addition, texture indices were calculated at five different spatial scales. The results showed that the 3×3 scale explained the largest proportion of deviance (see Table 7), making it ideal for the current sampling scale. (2) Scale dependence across study extents [66]. Our research was conducted at two spatial scales and across three areas, including the two smaller subareas—the Southeast and Northwest Areas—and the full Study Area. The results show that, regardless of the scale or area, the driving factors and their contributions to the patterns of community composition dissimilarity are inconsistent. Additionally, the predicted ecological distances also differ. (3) Consistency between study extent and explanatory variables. In large-scale GDM studies conducted at intercontinental scales, climatic factors are often the dominant predictors [16,41]. In contrast, small-scale studies, such as ours, require soil physicochemical properties to be used as explanatory variables. Only when the scale of the response variable aligns with that of the explanatory variables can the GDM yield interpretable results. This suggests that by linking variables appropriate to the scale, the GDM model can explain changes in species composition at a larger scale and is also fully applicable to analyzing the spatial patterns of species composition at smaller scales.

5. Conclusions

Based on the GDM results, our study demonstrates that, although plant community turnover across two spatial scales and three areas exhibited similar spatial patterns, the underlying drivers varied. AN was the primary factor explaining compositional dissimilarity in the Southeast Area, while SWC dominated in the Northwest Area and across the entire Study Area. Geographic distance consistently ranked second in all areas, and while texture indices explained less variation, they outperformed many vegetation indices and spectral bands, demonstrating their value as indicators of turnover under disturbance. These findings indicate that soil properties, geographic distance, and texture indices jointly influence species turnover, with their effects varying across scales and areas. Disturbances, including drought, grazing, tourism, and water-level variations in a nearby reservoir, altered turnover by modifying critical ecological drivers, either directly or indirectly. In combination with a comparative analysis of species IVs and ecological types, this study further confirms that the factors driving species turnover are shaped not only by scale but also by complex and diverse ecological processes acting at their respective scales. It also illustrates the potential of GDM for analyzing fine-scale species turnover patterns and the factors driving them in disturbed grasslands.

Author Contributions: Conceptualization, Z.W.; methodology: Z.W.; investigation, Z.W., Z.G., L.X., and S.Z.; data analysis, Z.W., Z.G., L.X., and S.Z.; writing—original draft preparation, Z.W., Z.G., L.X., and S.Z.; writing—review and editing: Z.W.; funding acquisition, Z.W. All authors have read and agreed to the published version of the manuscript.

Funding: This research was funded by the general research project of the Beijing Municipal Education Commission (KM201810028012).

Institutional Review Board Statement: Not applicable.

Data Availability Statement: Some of the data involved in this study are available upon request from the corresponding author.

Acknowledgments: We gratefully acknowledge the survey permit granted by the Yeyahu Wetland Nature Reserve during the research period, as well as their substantial support with transportation and access to the experimental sites. We also received invaluable support from Jianming Hong (College of Life Sciences) and Lin Zhu (College of Resources Environment and Tourism) of Capital

Normal University, who generously provided partial hardware and software resources, along with some technical assistance for this study.

Conflicts of Interest: The authors declare no conflicts of interest.

Appendix A

Table A1. Vegetation indices from WorldView-2 sensor spectral bands.

Vegetation Index	Abbreviation	Formulation	Type	Reference
Salinity Index_S1	S1	Blue/Red	A	[75]
Salinity Index_S2	S2	(Blue − Red)/(Blue + Red)	A	[75]
Salinity Index_S3	S3	(Green × Red)/Blue	A	[75]
Salinity Index_S5	S5	(Blue × Red)/Green	A	[75]
Salinity Index_S601	S601	(Red × NIR1)/Green	A	[75]
Salinity Index_S602	S602	(Red × NIR2)/Green	A	[75]
Salinity Index_1	Sal1	$(\text{Green} \times \text{Red})^{1/2}$	A	[76]
Salinity Index_201	Sal201	$(\text{Green}^2)^{1/2} + \text{Red}^2 + \text{NIR1}^2$	A	[77]
Salinity Index_202	Sal202	$(\text{Green}^2)^{1/2} + \text{Red}^2 + \text{NIR2}^2$	A	[77]
Salinity Index_3	Sal3	$(\text{Green}^2 + \text{Red}^2)^{1/2}$	A	[77]
Salinity Index_SI-T01	SI-T01	Red/NIR1 × 100	A	[78]
Salinity Index-SI-T02	SI-T01	Red/NIR2 × 100	A	[78]
Brightness Index_BI01	BI01	$(\text{NIR1}^2 + \text{Red}^2)^{1/2}$	A	[76]
Brightness Index-BI02	BI02	$(\text{NIR2}^2 + \text{Red}^2)^{1/2}$	A	[76]
Triangular Vegetation Index	TVI653	0.5 × (120 × (Red Edge − Green) − 200 × (Red − Green))	B	[79]
Structure-Insensitive Pigment Index	SIPI	(NIR1 − Blue)/(NIR1 − Red Edge)	B	[80]
RedEdge Simple Ratio Index	RE-SR 65	Red Edge/Red	B	[81]
Pigment-Specific Simple Ratio (Chlorophyll a)	PSSRa	NIR1/Red Edge	B	[82]
Pigment-Specific Simple Ratio (Chlorophyll b)	PSSRb	NIR1/Red	B	[82]
Carotenoid Reflectance Index	CRI	(1/Blue) − (1/Red Edge)	B	[83]
Transformed Chlorophyll Absorption in Reflectance Index	TCARI753	3 × [(NIR1 − Red) − 0.2 × (NIR1 − Green) × (NIR1/Red)]	B	[84]
Transformed Chlorophyll Absorption in Reflectance Index	TCARI	3 × [(Red Edge − Red) − 0.2 × (Red Edge − Green)(Red Edge/Red)]	B	[79]
Modified Chlorophyll Absorption in Reflectance Index	MCARI	[(Red Edge − Red) − 0.2 × (Red Edge − Green)] × (Red Edge/Red)	B	[85]
Modified Chlorophyll Absorption in Reflectance Index	MCARI753	[(NIR1 − Red) − 0.2(NIR1 − Green)] × (NIR1/Red)	B	[84]
Plant Senescence Reflectance Index	PSRI	(Red Edge − Blue)/NIR1	B	[86]
RedEdge Normalized Difference Vegetation Index	RE-NDVI65	(Red Edge − Red)/(Red Edge + Red)	B	[81]
Modified RedEdge Simple Ratio Index	mRE-SR651	(Red Edge − Coastal Blue)/(Red + Coastal Blue)	B	[81]
Simple Ratio Index_85	SRI85	NRI2/Red	C	[81]
Simple Ratio Index	SRI	NRI1/Red	C	[87]
Normalized Difference Vegetation Index	SRI84	NRI2/Yellow	C	[81]
RedEdge Normalized Difference Vegetation Index	RE-NDVI61	(Red Edge − Coastal Blue)/(Red Edge + Coastal Blue)	C	[81]
RedEdge Simple Ratio Index	RE-SR61	Red Edge/Coastal Blue	C	[79]

Table A1. *Cont.*

Vegetation Index	Abbreviation	Formulation	Type	Reference
Ratio Vegetation Index	RVI01	Red/NIR1	C	[88]
Ratio Vegetation Index	RVI02	NIR1/Red	C	[89]
Transformed Vegetation Index	TVI	$(NDVI + 0.5)^{1/2}$	C	[90]
Normalized Difference Index	NDI	(NIR1 − Red)/(NIR1 + Red)	C	[91]
Green Normalized Difference Vegetation Index	GNDVI	(NIR1 − Green)/(NIR1 + Green)	C	[89,92,93]
Green Normalized Difference Vegetation Index 2	GNDVI2	(NIR2 − Green)/(NIR2 + Green)	C	[94]
Modified Simple Ratio	MSR75	$[(NIR1/Red) - 1]/[(NIR1/Red)^{1/2} + 1]$	C	[84]
Modified Simple Ratio	MSR02	(NIR1 − Blue)/(Red − Blue)	C	[91]
Visible Green Index	VGI	(Green − Red)/(Green + Red)	C	[95]
Modified Normalized Difference	MND	(NIR1 − Blue)/(NIR1 + Red Edge − 2 × Blue)	C	[91]
Green Index	GI	(NIR1/Green) − 1	C	[83]
Red Index	RI	(NIR1/Red) − 1	C	[83]
Normalized Difference Red Edge index	NDRE	(NIR1 − Red Edge)/(NIR1 + Red Edge)	C	[96]
Renormalized Vegetation Index	RDVI	$(NIR1 - red)/(NIR1 + red)^{1/2}$	C	[89]
Normalized Difference Vegetation Index	NDVI	(NIR1 − Red)/(NIR1 + Red)	C	[97]
Normalized Difference Red Edge index 2	NDRE2	(NIR2 − Red Edge)/(NIR2 + Red Edge)	C	[94]
Normalized Difference Vegetation Index 2	NDVI202	(NIR2 − red)/(NIR2 + red)	C	[97]
NDVI 3		(NIR1−Yellow)/(NIR1 + Yellow)	C	[98]
NDVI 4		(Red Edge − Coastal Blue)/(Red Edge + Coastal Blue)	C	[98]
NDVI 5		(Red Edge − Red)/(Red Edge + Red)	C	[98]
NDVI 6		(NIR2 − Yellow)/(NIR2 + Yellow)	C	[81]
Generalized Difference VI	GDVI	$(NIR1^2 - Red^2)/(NIR1^2 + Red^2)$	C	[99]
Detection index	DI	NIR2/Red Edge	C	[100]
Normalized Difference Water Index01	NDWI01	(NIR1 − NIR2)/(NIR1 + NIR2)	C	[81,101,102]
Normalized Difference Water Index02	NDWI02	(Green − NIR2)/(Green + NIR2)	C	[103]
Optimized Soil-Adjusted Vegetation Index	OSAVI75	(1 + 0.6)(NIR1 − Red)/(NIR1 + Red + 0.16)	D	[79]
Modified Soil-Adjusted Vegetation Index	MSAVI	(1 + 0.5)(NIR1 − Red)/(NIR1 + Red + 0.5)	D	[104]
Soil-Adjusted VI01	Savi01	1.5 × (NIR1 − Red)/(NIR1 + Red + 0.5)	D	[105]
Soil-Adjusted VI02	Savi02	1.5 × (NIR2 − Red)/(NIR2 + Red + 0.5)	D	[105]
Soil–Adjusted VI 201	Savi201	1.5 × (NIR1 − Yellow)/(NIR1 + Yellow + 0.5)	D	[105]
Soil-Adjusted VI 202	Savi202	1.5 × (NIR2 − Yellow)/(NIR2 + Yellow + 0.5)	D	[105]
Enhanced Vegetation Index	EVI	2.5 × ((NIR1 − Red)/(NIR1 + 6 × Red − 7.5 × Blue + 1))	D	[106]
Atmospherically Resistant Vegetation Index	ARVI	(NIR2 − (2 × Red − Blue))/(NIR2 + (2 × Red − Blue))	D	[107]
Visible Atmospherically Resistant Index	VARI	(Green − Red)/(Green + Red − Blue)	D	[95]

Note: The Coastal, Blue, Green, Yellow, Red, Red Edge, NIR1, and NIR2 bands correspond to WorldView-2 bands 1 through 8, respectively, where category A represents vegetation indices related to soil salinity, category B includes indices associated with plant pigments and senescence, category C encompasses indices indicating vegetation growth and health, and category D consists of indices adjusted for soil background and atmospheric effects.

Table A2. Scientific names, IVs, and ecological types of the top 20 plant species in the Southeast Area.

Scientific Name	IV	Ecological Type
Artemisia tanacetifolia L.	12.17	Mesophytic
Artemisia lavandulaefolia DC.	8.66	Mesophytic
Gueldenstaedtia verna (Georgi) Boriss.	7.34	Mesophytic
Bothriochloa ischaemum (L.) Keng	6.77	Mesophytic
Hemarthria altissima (Poir.) Stapf et C. E. Hubb.	6.35	Hydrophytic
Scirpus planiculmis Fr.schmibt	6.01	Emergent
Lespedeza davurica (Laxm.) Schindl.	4.84	Mesophytic
Plantago asiatica L.	4.52	Mesophytic
Taraxacum brassicaefolium Kitag.	3.03	Mesophytic
Echinochloa crusgalli (L.) Beauv.	2.88	Mesophytic
Inula japonica Thunb.	2.41	Mesophytic
Plantago depressa Willd.	2.36	Mesophytic
Sphaerophysa salsula (Pall.) DC.	2.20	Halophytic
Chloris virgata Sw.	2.09	Mesophytic
Elymus dahuricus Turcz.	1.99	Halophytic
Sonchus wightianus DC.	1.98	Hydrophytic
Setaria viridis (L.) Beauv.	1.97	Mesophytic
Tournefortia sibirica L.	1.97	Mesophytic
Phragmites australis (Cav.) Trin. ex Steud.	1.92	Emergent
Ixeris chinensis (Thunb.) Nakai	1.81	Mesophytic

Table A3. Scientific names, IVs, and ecological types of the top 20 plant species in the Northwest Area.

Species Name	IV	Ecological Type
Hemarthria altissima (Poir.) Stapf et C. E. Hubb.	19.92	Hydrophytic
Scirpus planiculmis Fr.schmibt	14.21	Emergent
Artemisia tanacetifolia L.	10.76	Mesophytic
Inula japonica Thunb.	7.22	Mesophytic
Setaria viridis (L.) Beauv.	5.07	Mesophytic
Potentilla anserina L.	4.56	Halophytic
Artemisia lavandulaefolia DC.	4.50	Mesophytic
Echinochloa crusgalli (L.) Beauv.	3.50	Mesophytic
Plantago depressa Willd.	3.12	Mesophytic
Phragmites australis (Cav.) Trin. ex Steud.	2.54	Emergent
Typha angusitifolia L.	2.23	Emergent
Plantago major L.	1.94	Mesophytic
Typha davidiana (Kronf.) Hand. -Mazz	1.81	Emergent
Bothriochloa ischaemum (L.) Keng	1.69	Mesophytic
Elymus dahuricus Turcz.	1.63	Halophytic
Plantago asiatica L.	1.54	Mesophytic
Potentilla chinensis Ser.	1.03	Mesophytic
Equisetum palustre L.	0.96	Hydrophytic
Xanthium strumarium L.	0.96	Mesophytic
Lespedeza davurica (Laxm.) Schindl.	0.89	Mesophytic

Table A4. Scientific names, IVs, and ecological types of the top 20 plant species in the Study Area.

Scientific Name	IV	Ecological Type
Scirpus planiculmis Fr.schmibt	14.99	Emergent
Hemarthria altissima (Poir.) Stapf et C. E. Hubb.	14.19	Hydrophytic
Artemisia tanacetifolia L.	12.03	Mesophytic
Artemisia lavandulaefolia DC.	5.95	Mesophytic
Inula japonica Thunb.	4.28	Mesophytic
Bothriochloa ischaemum (L.) Keng	4.25	Mesophytic
Apocynum venetum L.	3.33	Halophytic
Setaria viridis (L.) Beauv.	3.22	Mesophytic
Echinochloa crusgalli (L.) Beauv.	2.96	Mesophytic
Plantago asiatica L.	2.93	Mesophytic
Gueldenstaedtia verna (Georgi) Boriss.	2.86	Mesophytic
Potentilla anserina L.	2.83	Halophytic
Plantago depressa Willd.	2.52	Mesophytic
Lespedeza davurica (Laxm.) Schindl.	2.05	Mesophytic
Phragmites australis (Cav.) Trin. ex Steud.	1.89	Emergent
Elymus dahuricus Turcz.	1.82	Halophytic
Taraxacum brassicaefolium Kitag.	1.35	Mesophytic
Chloris virgata Sw.	1.14	Mesophytic

Table A4. *Cont.*

Scientific Name	IV	Ecological Type
Typha angusitifolia L.	1.06	Emergent
Plantago major L.	1.04	Mesophytic

References

1. Legendre, P.; De Cáceres, M. Beta Diversity as the Variance of Community Data: Dissimilarity Coefficients and Partitioning. *Ecol. Lett.* **2013**, *16*, 951–963. [CrossRef]
2. Whittaker, R.H. Evolution and Measurement of Species Diversity. *TAXON* **1972**, *21*, 213–251. [CrossRef]
3. Rosenzweig, M.L. *Species Diversity in Space and Time*; Cambridge University Press: Cambridge, UK, 1995; ISBN 978-0-511-62338-7.
4. Cody, M.L. Towards a Theory of Continental Species Diversities: Bird Distributions Over Mediterranean Habitat Gradients. In *Ecology and Evolution of Communities*; Cody, M.L., Diamond, J.M., Eds.; Belknap Press: Cambridge, MA, USA, 1975; pp. 214–257. ISBN 978-0-674-22444-5.
5. Magurran, A.E.; McGill, B.J. *Biological Diversity: Frontiers in Measurement and Assessment*; Oxford University Press: Oxford, UK, 2011; ISBN 978-0-19-958066-8.
6. Si, X.; Zhao, Y.; Chen, C.; Ren, P.; Zeng, D.; Wu, L.; Ding, P. Beta-diversity partitioning: Methods, applications and perspectives. *Biodivers. Sci.* **2017**, *25*, 464–480. [CrossRef]
7. Baselga, A. The Relationship between Species Replacement, Dissimilarity Derived from Nestedness, and Nestedness. *Glob. Ecol. Biogeogr.* **2012**, *21*, 1223–1232. [CrossRef]
8. Sabatini, F.M.; Jiménez-Alfaro, B.; Jandt, U.; Chytrý, M.; Field, R.; Kessler, M.; Lenoir, J.; Schrodt, F.; Wiser, S.K.; Arfin Khan, M.A.S.; et al. Global Patterns of Vascular Plant Alpha Diversity. *Nat. Commun.* **2022**, *13*, 4683. [CrossRef] [PubMed]
9. Večeřa, M.; Divíšek, J.; Lenoir, J.; Jiménez-Alfaro, B.; Biurrun, I.; Knollová, I.; Agrillo, E.; Campos, J.A.; Čarni, A.; Crespo Jiménez, G.; et al. Alpha Diversity of Vascular Plants in European Forests. *J. Biogeogr.* **2019**, *46*, 1919–1935. [CrossRef]
10. Dalmayne, J.; Möckel, T.; Prentice, H.C.; Schmid, B.C.; Hall, K. Assessment of Fine-Scale Plant Species Beta Diversity Using WorldView-2 Satellite Spectral Dissimilarity. *Ecol. Inform.* **2013**, *18*, 1–9. [CrossRef]
11. Clarke, K.R.; Somerfield, P.J.; Chapman, M.G. On Resemblance Measures for Ecological Studies, Including Taxonomic Dissimilarities and a Zero-Adjusted Bray–Curtis Coefficient for Denuded Assemblages. *J. Exp. Mar. Biol. Ecol.* **2006**, *330*, 55–80. [CrossRef]
12. Mokany, K.; Ware, C.; Woolley, S.N.C.; Ferrier, S.; Fitzpatrick, M.C. A Working Guide to Harnessing Generalized Dissimilarity Modelling for Biodiversity Analysis and Conservation Assessment. *Glob. Ecol. Biogeogr.* **2022**, *31*, 802–821. [CrossRef]
13. McKnight, M.W.; White, P.S.; McDonald, R.I.; Lamoreux, J.F.; Sechrest, W.; Ridgely, R.S.; Stuart, S.N. Putting Beta-Diversity on the Map: Broad-Scale Congruence and Coincidence in the Extremes. *PLoS Biol.* **2007**, *5*, e272. [CrossRef]
14. Socolar, J.B.; Gilroy, J.J.; Kunin, W.E.; Edwards, D.P. How Should Beta-Diversity Inform Biodiversity Conservation? *Trends Ecol. Evol.* **2016**, *31*, 67–80. [CrossRef]
15. Gossner, M.M.; Lewinsohn, T.M.; Kahl, T.; Grassein, F.; Boch, S.; Prati, D.; Birkhofer, K.; Renner, S.C.; Sikorski, J.; Wubet, T.; et al. Land-Use Intensification Causes Multitrophic Homogenization of Grassland Communities. *Nature* **2016**, *540*, 266–269. [CrossRef] [PubMed]
16. He, J.; Lin, S.; Kong, F.; Yu, J.; Zhu, H.; Jiang, H. Determinants of the Beta Diversity of Tree Species in Tropical Forests: Implications for Biodiversity Conservation. *Sci. Total Environ.* **2020**, *704*, 135301. [CrossRef] [PubMed]
17. Nekola, J.C.; White, P.S. The Distance Decay of Similarity in Biogeography and Ecology. *J. Biogeogr.* **1999**, *26*, 867–878. [CrossRef]
18. Martín-Devasa, R.; Martínez-Santalla, S.; Gómez-Rodríguez, C.; Crujeiras, R.M.; Baselga, A. Species Range Size Shapes Distance-decay in Community Similarity. *Divers. Distrib.* **2022**, *28*, 1348–1357. [CrossRef]
19. Vega, E.; Martínez-Ramos, M.; García-Oliva, F.; Oyama, K. Influence of Environmental Heterogeneity and Geographic Distance on Beta-Diversity of Woody Communities. *Plant Ecol.* **2020**, *221*, 595–614. [CrossRef]
20. Qian, H.; Ricklefs, R.E. Disentangling the Effects of Geographic Distance and Environmental Dissimilarity on Global Patterns of Species Turnover. *Glob. Ecol. Biogeogr.* **2012**, *21*, 341–351. [CrossRef]
21. Saito, V.S.; Soininen, J.; Fonseca-Gessner, A.A.; Siqueira, T. Dispersal Traits Drive the Phylogenetic Distance Decay of Similarity in Neotropical Stream Metacommunities. *J. Biogeogr.* **2015**, *42*, 2101–2111. [CrossRef]
22. König, C.; Weigelt, P.; Kreft, H. Dissecting Global Turnover in Vascular Plants. *Glob. Ecol. Biogeogr.* **2017**, *26*, 228–242. [CrossRef]
23. Qian, H. Beta Diversity in Relation to Dispersal Ability for Vascular Plants in North America. *Glob. Ecol. Biogeogr.* **2009**, *18*, 327–332. [CrossRef]
24. Palmer, M.W. Distance Decay in an Old-growth Neotropical Forest. *J. Veg. Sci.* **2005**, *16*, 161–166. [CrossRef]

25. La Sorte, F.A.; McKinney, M.L.; Pyšek, P.; Klotz, S.; Rapson, G.L.; Celesti-Grapow, L.; Thompson, K. Distance Decay of Similarity among European Urban Floras: The Impact of Anthropogenic Activities on β Diversity. *Glob. Ecol. Biogeogr.* **2008**, *17*, 363–371. [CrossRef]
26. Steinbauer, M.J.; Dolos, K.; Reineking, B.; Beierkuhnlein, C. Current Measures for Distance Decay in Similarity of Species Composition Are Influenced by Study Extent and Grain Size. *Glob. Ecol. Biogeogr.* **2012**, *21*, 1203–1212. [CrossRef]
27. Carvalho, J.C.; Cardoso, P.; Gomes, P. Determining the Relative Roles of Species Replacement and Species Richness Differences in Generating Beta-diversity Patterns. *Glob. Ecol. Biogeogr.* **2012**, *21*, 760–771. [CrossRef]
28. Baselga, A. Disentangling Distance Decay of Similarity from Richness Gradients: Response to Soininen et al. 2007. *Ecography* **2007**, *30*, 838–841. [CrossRef]
29. Peguero, G.; Ferrín, M.; Sardans, J.; Verbruggen, E.; Ramírez-Rojas, I.; Van Langenhove, L.; Verryckt, L.T.; Murienne, J.; Iribar, A.; Zinger, L.; et al. Decay of Similarity across Tropical Forest Communities: Integrating Spatial Distance with Soil Nutrients. *Ecology* **2022**, *103*, e03599. [CrossRef]
30. Graco-Roza, C.; Aarnio, S.; Abrego, N.; Acosta, A.T.R.; Alahuhta, J.; Altman, J.; Angiolini, C.; Aroviita, J.; Attorre, F.; Baastrup-Spohr, L.; et al. Distance Decay 2.0—A Global Synthesis of Taxonomic and Functional Turnover in Ecological Communities. *Glob. Ecol. Biogeogr.* **2022**, *31*, 1399–1421. [CrossRef]
31. Rocchini, D. Distance Decay in Spectral Space in Analysing Ecosystem B-diversity. *Int. J. Remote Sens.* **2007**, *28*, 2635–2644. [CrossRef]
32. Kim, D.; Shin, Y.H. Spatial Autocorrelation Potentially Indicates the Degree of Changes in the Predictive Power of Environmental Factors for Plant Diversity. *Ecol. Indic.* **2016**, *60*, 1130–1141. [CrossRef]
33. Rocchini, D.; Cade, B.S. Quantile Regression Applied to Spectral Distance Decay. *IEEE Geosci. Remote Sens. Lett.* **2008**, *5*, 640–643. [CrossRef]
34. Tuomisto, H.; Poulsen, A.D.; Ruokolainen, K.; Moran, R.C.; Quintana, C.; Celi, J.; Cañas, G. Linking Floristic Patterns with Soil Heterogeneity and Satellite Imagery in Ecuadorian Amazonia. *Ecol. Appl.* **2003**, *13*, 352–371. [CrossRef]
35. Ribeiro, I.; Proença, V.; Serra, P.; Palma, J.; Domingo-Marimon, C.; Pons, X.; Domingos, T. Remotely Sensed Indicators and Open-Access Biodiversity Data to Assess Bird Diversity Patterns in Mediterranean Rural Landscapes. *Sci. Rep.* **2019**, *9*, 6826. [CrossRef] [PubMed]
36. Wang, X.; Van Nostrand, J.D.; Deng, Y.; Lü, X.; Wang, C.; Zhou, J.; Han, X. Scale-Dependent Effects of Climate and Geographic Distance on Bacterial Diversity Patterns across Northern China's Grasslands. *FEMS Microbiol. Ecol.* **2015**, *91*, fiv133. [CrossRef] [PubMed]
37. Qian, H.; Shimono, A. Effects of Geographic Distance and Climatic Dissimilarity on Species Turnover in Alpine Meadow Communities across a Broad Spatial Extent on the Tibetan Plateau. *Plant Ecol.* **2012**, *213*, 1357–1364. [CrossRef]
38. Feng, M.; Tripathi, B.M.; Shi, Y.; Adams, J.M.; Zhu, Y.; Chu, H. Interpreting Distance-decay Pattern of Soil Bacteria via Quantifying the Assembly Processes at Multiple Spatial Scales. *MicrobiologyOpen* **2019**, *8*, e00851. [CrossRef]
39. Qian, H.; Ricklefs, R.E.; White, P.S. Beta Diversity of Angiosperms in Temperate Floras of Eastern Asia and Eastern North America. *Ecol. Lett.* **2005**, *8*, 15–22. [CrossRef]
40. Buckley, L.B.; Jetz, W. Linking Global Turnover of Species and Environments. *Proc. Natl. Acad. Sci. USA* **2008**, *105*, 17836–17841. [CrossRef]
41. Fitzpatrick, M.C.; Sanders, N.J.; Normand, S.; Svenning, J.-C.; Ferrier, S.; Gove, A.D.; Dunn, R.R. Environmental and Historical Imprints on Beta Diversity: Insights from Variation in Rates of Species Turnover along Gradients. *Proc. R. Soc. B* **2013**, *280*, 20131201. [CrossRef]
42. Ferrier, S.; Manion, G.; Elith, J.; Richardson, K. Using Generalized Dissimilarity Modelling to Analyse and Predict Patterns of Beta Diversity in Regional Biodiversity Assessment. *Divers. Distrib.* **2007**, *13*, 252–264. [CrossRef]
43. Ferrier, S.; Powell, G.V.N.; Richardson, K.S.; Manion, G.; Overton, J.M.; Allnutt, T.F.; Cameron, S.E.; Mantle, K.; Burgess, N.D.; Faith, D.P.; et al. Mapping More of Terrestrial Biodiversity for Global Conservation Assessment. *BioScience* **2004**, *54*, 1101. [CrossRef]
44. Oksanen, J.; Tonteri, T. Rate of Compositional Turnover along Gradients and Total Gradient Length. *J. Veg. Sci.* **1995**, *6*, 815–824. [CrossRef]
45. Ferrier, S. Mapping Spatial Pattern in Biodiversity for Regional Conservation Planning: Where to from Here? *Syst. Biol.* **2002**, *51*, 331–363. [CrossRef] [PubMed]
46. Fitzpatrick, M.C.; Mokany, K.; Manion, G.; Nieto-Lugilde, D.; Ferrier, S. gdm: Generalized Dissimilarity Modeling. Reference Manual. R Package Version 1.6.0-7. 2025. Available online: https://cran.r-project.org/web/packages/gdm/gdm.pdf (accessed on 5 November 2025).
47. Lasram, F.B.R.; Hattab, T.; Halouani, G.; Romdhane, M.S.; Le Loc'h, F. Modeling of Beta Diversity in Tunisian Waters: Predictions Using Generalized Dissimilarity Modeling and Bioregionalisation Using Fuzzy Clustering. *PLoS ONE* **2015**, *10*, e0131728. [CrossRef] [PubMed]

48. Fitzpatrick, M.C.; Sanders, N.J.; Ferrier, S.; Longino, J.T.; Weiser, M.D.; Dunn, R. Forecasting the Future of Biodiversity: A Test of Single- and Multi-Species Models for Ants in North America. *Ecography* **2011**, *34*, 836–847. [CrossRef]
49. Bush, A.; Catullo, R.; Mokany, K.; Harwood, T.; Hoskins, A.J.; Ferrier, S. Incorporating Existing Thermal Tolerance into Projections of Compositional Turnover under Climate Change. *Glob. Ecol. Biogeogr.* **2019**, *28*, 851–861. [CrossRef]
50. Liu, K.; Zhao, W.; Guo, X.; Hu, D.; Gong, Z.; Long, J. Spectral Bands of Typical Wetland Vegetation in the W Ild Duck Lake. *Acta Ecol. Sin.* **2010**, *30*, 5853–5861.
51. Gong, Z.; Zhao, W.; Hu, D. Wetland Plant Community Characteristics and Ecological Succession Mode in Wild Duck Lake along Salt and Water Environment Gradient. *Prog. Nat. Sci.* **2009**, *19*, 1272–1280.
52. Duan, T.; Zhang, J.; Wang, Z. Responses and Indicators of Composition, Diversity, and Productivity of Plant Communities at Different Levels of Disturbance in a Wetland Ecosystem. *Diversity* **2021**, *13*, 252. [CrossRef]
53. Bao, S. *Soil and Agricultural Chemistry Analysis*, 3rd ed.; China Agricultural Press: Beijing, China, 2000; ISBN 978-7-109-06644-1.
54. Xie, X. *Soil and Plant Nutrition Experiment*, 1st ed.; Zhejiang University Press: Hangzhou, China, 2014; ISBN 7-308-13552-7.
55. Guo, Y.; Dai, J.; Feng, H.; Lu, Y.; Jia, C.; Chen, C.; Xiong, F. Standard mapping of soil textural triangle and automatic query of soil texture classes. *Acta Pedol. Sin.* **2013**, *50*, 1221–1225. [CrossRef]
56. Hill, M.J. Vegetation Index Suites as Indicators of Vegetation State in Grassland and Savanna: An Analysis with Simulated SENTINEL 2 Data for a North American Transect. *Remote Sens. Environ.* **2013**, *137*, 94–111. [CrossRef]
57. John, R.; Chen, J.; Lu, N.; Guo, K.; Liang, C.; Wei, Y.; Noormets, A.; Ma, K.; Han, X. Predicting Plant Diversity Based on Remote Sensing Products in the Semi-Arid Region of Inner Mongolia. *Remote Sens. Environ.* **2008**, *112*, 2018–2032. [CrossRef]
58. Tian, Y.; Fu, G. Quantifying Plant Species α-Diversity Using Normalized Difference Vegetation Index and Climate Data in Alpine Grasslands. *Remote Sens.* **2022**, *14*, 5007. [CrossRef]
59. Fang, J.; Wang, X.; Shen, Z.; Tang, Z.; He, J.; Yu, D.; Jiang, Y.; Wang, Z.; Zheng, C.; Zhu, J.; et al. Methods and protocols for plant community inventory. *Biodivers. Sci.* **2009**, *17*, 533. [CrossRef]
60. Gong, Z.; Gong, H.; Hu, D. *Wetland Plants in Wild Duke Lake, Beijing*, 1st ed.; China Environmental Science Press: Beijing, China, 2012; ISBN 978-7-5111-0953-8.
61. Bray, J.R.; Curtis, J.T. An Ordination of the Upland Forest Communities of Southern Wisconsin. *Ecol. Monogr.* **1957**, *27*, 325–349. [CrossRef]
62. Dormann, C.F.; Elith, J.; Bacher, S.; Buchmann, C.; Carl, G.; Carré, G.; Marquéz, J.R.G.; Gruber, B.; Lafourcade, B.; Leitão, P.J.; et al. Collinearity: A Review of Methods to Deal with It and a Simulation Study Evaluating Their Performance. *Ecography* **2013**, *36*, 27–46. [CrossRef]
63. Xu, J.; Zhao, L.; Lin, Q. *Wetland Plants in Beijing*, 1st ed.; Beijing Science and Technology Press: Beijing, China, 2009; ISBN 978-7-5304-4532-7.
64. Li, Y.; Liu, F.; Zhou, Y.; Liu, X.; Wang, Q. Large-Scale Geographic Patterns and Environmental and Anthropogenic Drivers of Wetland Plant Diversity in the Qinghai-Tibet Plateau. *BMC Ecol. Evo* **2024**, *24*, 74. [CrossRef]
65. Polley, H.W.; Yang, C.; Wilsey, B.J.; Fay, P.A. Spectral Heterogeneity Predicts Local-Scale Gamma and Beta Diversity of Mesic Grasslands. *Remote Sens.* **2019**, *11*, 458. [CrossRef]
66. Ibanez, T.; Keppel, G.; Baider, C.; Birkinshaw, C.; Culmsee, H.; Cordell, S.; Florens, F.B.V.; Franklin, J.; Giardina, C.P.; Gillespie, T.W.; et al. Regional Forcing Explains Local Species Diversity and Turnover on Tropical Islands. *Glob. Ecol. Biogeogr.* **2018**, *27*, 474–486. [CrossRef]
67. Cavender-Bares, J.; Schneider, F.D.; Santos, M.J.; Armstrong, A.; Carnaval, A.; Dahlin, K.M.; Fatoyinbo, L.; Hurtt, G.C.; Schimel, D.; Townsend, P.A.; et al. Integrating Remote Sensing with Ecology and Evolution to Advance Biodiversity Conservation. *Nat. Ecol. Evol.* **2022**, *6*, 506–519. [CrossRef]
68. Pettorelli, N.; Nagendra, H.; Rocchini, D.; Rowcliffe, M.; Williams, R.; Ahumada, J.; De Angelo, C.; Atzberger, C.; Boyd, D.; Buchanan, G.; et al. Remote Sensing in Ecology and Conservation: Three Years On. *Remote Sens. Ecol. Conserv.* **2017**, *3*, 53–56. [CrossRef]
69. Lechner, A.M.; Foody, G.M.; Boyd, D.S. Applications in Remote Sensing to Forest Ecology and Management. *One Earth* **2020**, *2*, 405–412. [CrossRef]
70. Wang, Z.; Ma, Y.; Zhang, Y.; Shang, J. Review of Remote Sensing Applications in Grassland Monitoring. *Remote Sens.* **2022**, *14*, 2903. [CrossRef]
71. Jiménez-Alfaro, B.; Suárez-Seoane, S.; Chytrý, M.; Hennekens, S.M.; Willner, W.; Hájek, M.; Agrillo, E.; Álvarez-Martínez, J.M.; Bergamini, A.; Brisse, H.; et al. Modelling the Distribution and Compositional Variation of Plant Communities at the Continental Scale. *Divers. Distrib.* **2018**, *24*, 978–990. [CrossRef]
72. Keil, P.; Schweiger, O.; Kühn, I.; Kunin, W.E.; Kuussaari, M.; Settele, J.; Henle, K.; Brotons, L.; Pe'er, G.; Lengyel, S.; et al. Patterns of Beta Diversity in Europe: The Role of Climate, Land Cover and Distance across Scales. *J. Biogeogr.* **2012**, *39*, 1473–1486. [CrossRef]

73. Wulder, M.A.; White, J.C.; Coops, N.C.; Butson, C.R. Multi-Temporal Analysis of High Spatial Resolution Imagery for Disturbance Monitoring. *Remote Sens. Environ.* **2008**, *112*, 2729–2740. [CrossRef]
74. Stuckenberg, T.; Münch, Z.; van Niekerk, A. Multi-Temporal Remote Sensing Land-Cover Change Detection for Biodiversity Assessment in the Berg River Catchment. *South Afr. J. Geomat.* **2013**, *2*, 189–205.
75. Abbas, A.; Khan, S. Using Remote Sensing Techniques for Appraisal of Irrigated Soil Salinity. In Proceedings of the International Congress on Modelling and Simulation. (MODSIM 2007), Modelling and Simulation Society of Australia and New Zealand, Christchurch, New Zealand, 10–13 December 2007; pp. 2632–2638.
76. Khan, N.M.; Rastoskuev, V.V.; Shalina, E.V.; Sato, Y. Mapping Salt-Affected Soils Using Remote Sensing Indicators—A Simple Approach with the Use of GIS IDRISI. In Proceedings of the 22nd Asian Conference on Remote Sensing, Singapore, 5 November 2001; pp. 5–9.
77. Douaoui, A.E.K.; Nicolas, H.; Walter, C. Detecting Salinity Hazards within a Semiarid Context by Means of Combining Soil and Remote-Sensing Data. *Geoderma* **2006**, *134*, 217–230. [CrossRef]
78. Tripathi, N.K.; Rai, B.K.; Dwivedi, P. Spatial Modelling of Soil Alkalinity in GIS Environment Using IRS Data. In Proceedings of the 18th Asian Conference on Remote Sensing, Kuala Lumpur, Malaysia, 20–25 October 1997; pp. 81–86.
79. Haboudane, D.; Miller, J.R.; Tremblay, N.; Zarco-Tejada, P.J.; Dextraze, L. Integrated Narrow-Band Vegetation Indices for Prediction of Crop Chlorophyll Content for Application to Precision Agriculture. *Remote Sens. Environ.* **2002**, *81*, 416–426. [CrossRef]
80. Peluelas, J.; Baret, F.; Filella, I. Semi-Empirical Indices to Assess Carotenoids/Chlorophyll a Ratio from Leaf Spectral Reflectance. *Photosynthetica* **1995**, *31*, 221–230.
81. Pu, R.; Landry, S. A Comparative Analysis of High Spatial Resolution IKONOS and WorldView-2 Imagery for Mapping Urban Tree Species. *Remote Sens. Environ.* **2012**, *124*, 516–533. [CrossRef]
82. Blackburn, G.A. Spectral Indices for Estimating Photosynthetic Pigment Concentrations: A Test Using Senescent Tree Leaves. *Int. J. Remote Sens.* **1998**, *19*, 657–675. [CrossRef]
83. Gitelson, A.A.; Viña, A.; Ciganda, V.; Rundquist, D.C.; Arkebauer, T.J. Remote Estimation of Canopy Chlorophyll Content in Crops. *Geophys. Res. Lett.* **2005**, *32*, 2005GL022688. [CrossRef]
84. Peña-Barragán, J.M.; Ngugi, M.K.; Plant, R.E.; Six, J. Object-Based Crop Identification Using Multiple Vegetation Indices, Textural Features and Crop Phenology. *Remote Sens. Environ.* **2011**, *115*, 1301–1316. [CrossRef]
85. Daughtry, C. Estimating Corn Leaf Chlorophyll Concentration from Leaf and Canopy Reflectance. *Remote Sens. Environ.* **2000**, *74*, 229–239. [CrossRef]
86. Merzlyak, M.N.; Gitelson, A.A.; Chivkunova, O.B.; Rakitin, V.Y. Non-destructive Optical Detection of Pigment Changes during Leaf Senescence and Fruit Ripening. *Physiol. Plant.* **1999**, *106*, 135–141. [CrossRef]
87. Jordan, C.F. Derivation of Leaf-Area Index from Quality of Light on the Forest Floor. *Ecology* **1969**, *50*, 663–666. [CrossRef]
88. Richardson, A.J.; Weigand, C. Distinguishing Vegetation from Soil Background Information. *Photogramm. Eng. Remote Sens.* **1977**, *43*, 1541–1552.
89. Li, X.; Zhang, Y.; Bao, Y.; Luo, J.; Jin, X.; Xu, X.; Song, X.; Yang, G. Exploring the Best Hyperspectral Features for LAI Estimation Using Partial Least Squares Regression. *Remote Sens.* **2014**, *6*, 6221–6241. [CrossRef]
90. Deering, D.; Rouse, J. Measuring "Forage Production" of Grazing Units from Landsat MSS Data. In Proceedings of the 10th International Symposium on Remote Sensing of Environment, Ann Arbor, MI, USA, 6–10 October 1975; pp. 1169–1178.
91. Sims, D.A.; Gamon, J.A. Relationships between Leaf Pigment Content and Spectral Reflectance across a Wide Range of Species, Leaf Structures and Developmental Stages. *Remote Sens. Environ.* **2002**, *81*, 337–354. [CrossRef]
92. Ahamed, T.; Tian, L.; Zhang, Y.; Ting, K.C. A Review of Remote Sensing Methods for Biomass Feedstock Production. *Biomass Bioenergy* **2011**, *35*, 2455–2469. [CrossRef]
93. Gitelson, A.A.; Kaufman, Y.J.; Merzlyak, M.N. Use of a Green Channel in Remote Sensing of Global Vegetation from EOS-MODIS. *Remote Sens. Environ.* **1996**, *58*, 289–298. [CrossRef]
94. Mutanga, O.; Adam, E.; Cho, M.A. High Density Biomass Estimation for Wetland Vegetation Using WorldView-2 Imagery and Random Forest Regression Algorithm. *Int. J. Appl. Earth Obs. Geoinf.* **2012**, *18*, 399–406. [CrossRef]
95. Gitelson, A.A.; Kaufman, Y.J.; Stark, R.; Rundquist, D. Novel Algorithms for Remote Estimation of Vegetation Fraction. *Remote Sens. Environ.* **2002**, *80*, 76–87. [CrossRef]
96. Barnes, E.M.; Clarke, T.R.; Richards, S.E.; Colaizzi, P.D.; Haberland, J.; Kostrzewski, M.; Waller, P.; Choi, C.; Riley, E.; Thompson, T. Coincident Detection of Crop Water Stress, Nitrogen Status and Canopy Density Using Ground-Based Multispectral Data. In Proceedings of the Fifth International Conference on Precision Agriculture, Bloomington, MN, USA, 16 July 2000.
97. Abood, S.; Maclean, A.; Falkowski, M. *Soil Salinity Detection in the Mesopotamian Agricultural Plain Utilizing WorldView-2 Imagery*; Michigan Technological University: Houghton, MI, USA, 2011.
98. Nouri, H.; Beecham, S.; Anderson, S.; Nagler, P. High Spatial Resolution WorldView-2 Imagery for Mapping NDVI and Its Relationship to Temporal Urban Landscape Evapotranspiration Factors. *Remote Sens.* **2014**, *6*, 580–602. [CrossRef]

99. Wu, W.; Mhaimeed, A.S.; Al-Shafie, W.M.; Ziadat, F.; Dhehibi, B.; Nangia, V.; De Pauw, E. Mapping Soil Salinity Changes Using Remote Sensing in Central Iraq. *Geoderma Reg.* **2014**, *2–3*, 21–31. [CrossRef]
100. Alexakis, D.D.; Daliakopoulos, I.N.; Panagea, I.S.; Tsanis, I.K. Assessing Soil Salinity Using WorldView-2 Multispectral Images in Timpaki, Crete, Greece. *Geocarto Int.* **2018**, *33*, 321–338. [CrossRef]
101. Gao, B. NDWI—A Normalized Difference Water Index for Remote Sensing of Vegetation Liquid Water from Space. *Remote Sens. Environ.* **1996**, *58*, 257–266. [CrossRef]
102. Hartling, S.; Sagan, V.; Sidike, P.; Maimaitijiang, M.; Carron, J. Urban Tree Species Classification Using a WorldView-2/3 and LiDAR Data Fusion Approach and Deep Learning. *Sensors* **2019**, *19*, 1284. [CrossRef]
103. Chen, Z.; Ning, X.; Zhang, J. Urban Land Cover Classification Based on WorldView-2 Image Data. In Proceedings of the 2012 International Symposium on Geomatics for Integrated Water Resource Management, Lanzhou, China, 19–21 October 2012; IEEE: New York, NY, USA, 2012; pp. 1–5.
104. Qi, J.; Chehbouni, A.; Huete, A.R.; Kerr, Y.H.; Sorooshian, S. A Modified Soil Adjusted Vegetation Index. *Remote Sens. Environ.* **1994**, *48*, 119–126. [CrossRef]
105. Muller, S.J.; Van Niekerk, A. Identification of WorldView-2 Spectral and Spatial Factors in Detecting Salt Accumulation in Cultivated Fields. *Geoderma* **2016**, *273*, 1–11. [CrossRef]
106. Huete, A.; Justice, C.; van Leeuwen, W. *MODIS Vegetation Index (MOD13) Algorithm Theoretical Basis Document, Version 3*; University of Arizona: Tucson, AZ, USA, 1999. Available online: https://modis.gsfc.nasa.gov/data/atbd/atbd_mod13.pdf (accessed on 5 November 2025).
107. Kaufman, Y.J.; Tanre, D. Atmospherically Resistant Vegetation Index (ARVI) for EOS-MODIS. *IEEE Trans. Geosci. Remote Sens.* **1992**, *30*, 261–270. [CrossRef]

Disclaimer/Publisher's Note: The statements, opinions and data contained in all publications are solely those of the individual author(s) and contributor(s) and not of MDPI and/or the editor(s). MDPI and/or the editor(s) disclaim responsibility for any injury to people or property resulting from any ideas, methods, instructions or products referred to in the content.